

Gamma-ray and Synchrotron Radiation from Dark Matter annihilations in Ultra-faint Dwarf Galaxies

Pooja Bhattacharjee^a Debajyoti Choudhury^b Kasinath Das^c
Dilip Kumar Ghosh^c and Pratik Majumdar^d

^aDepartment of Physics, Bose Institute, EN-80, Sector V, Bidhannagar, Kolkata - 700091, India

^bDepartment of Physics and Astrophysics, University of Delhi, Delhi 110 007, India.

^cSchool of Physical Sciences, Indian Association for the Cultivation of Science, 2A & 2B Raja S C Mullick Road, Kolkata 700 032, India.

^dAstroparticle Physics and Cosmology Division, HBNI, Saha Institute of Nuclear Physics, 1/AF Bidhan Nagar, Kolkata 700 064, India.

E-mail: pooja.bhattacharjee06@gmail.com, debajyoti.choudhury@gmail.com,
tpkd@iacs.res.in, kasinath.das91@gmail.com, tpdkg@iacs.res.in,
majumdar.mpratik@gmail.com

Abstract. The very large (100-1000) mass-to-light ratio applicable to the ultra-faint dwarf galaxies (UFDs) implies a high concentration of dark matter, thus rendering them ideal theatres for indirect signatures of dark matter. In this paper, we consider 14 recently discovered UFDs and study the electromagnetic radiation emanating from them over a wide range, from gamma ray down to radio frequencies. We analyze the Fermi-LAT data on high energy gamma rays and radio fluxes at the GMRT and VLA to obtain upper limits on annihilation cross section $\langle\sigma v\rangle$ in a model independent way. We further discuss the sensitivity of the Square Kilometer Array radio telescope in probing the synchrotron radiation from the aforementioned UFDs. We also investigate the dependences of the said upper limits on the uncertainties in the determination of various astrophysical parameters.

Keywords: dark Matter theory, dwarf galaxies, gamma ray theory, dark matter experiments

Contents

1	Introduction	1
2	γ-ray flux from pair-annihilation of WIMPs	5
2.1	Astrophysical Factor (J)	6
2.2	Dependence of J on the density profiles	9
3	Analysis of γ-ray fluxes from ultra-faint dwarf galaxies	11
3.1	Constraints on DM annihilation with eleven years of Fermi-LAT data	12
3.2	Comparison between our obtained result from the Fermi-LAT analysis with the estimated limits provided by Planck	15
4	Synchrotron radiation from ultra-faint dwarf galaxies	16
4.1	Results pertaining to the Ultra Faint Dwarf Galaxies	20
4.2	Future projections	23
5	Astrophysical Uncertainties and the Constraints	23
5.1	Uncertainties in the Gamma-Ray bounds	24
5.2	Uncertainties in the synchrotron fluxes	26
6	Discussions and Conclusions	29
A	Source details	34
B	Parameters used in Science Tools	36

1 Introduction

The presence of an abundant non-baryonic dark matter (DM) component in our universe has not only been established through a variety of independent observations[1], but is also expected to have played a key role in the evolution of structure at a multitude of scales[2]. While a particulate nature of the DM is called for, such an interpretation necessitates physics beyond the Standard Model (SM) not only in terms of the identity of the said particle, but also in terms of the dynamics that determines its relic density. Several different classes of scenarios have been proposed with the WIMP (Weakly Interacting Massive Particles) paradigm being one of the most theoretically appealing ones. This is so because not only are the parameters (masses and couplings) naturally at the electroweak scale, but the very interaction that decides the relic density of the DM particle χ (largely through processes like $\chi\chi \rightarrow \mathcal{SS}$, where

\mathcal{S} is a generic SM field) would also render amenable their detection in terrestrial experiments [3–5]. While much effort has gone into theoretical studies that seek to reproduce a relic density commensurate with what the cosmological data suggests, unfortunately no confirmatory signals have been seen in any laboratory experiments. These include not only dedicated *Direct Search* experiments (based on $\chi\mathcal{S} \rightarrow \chi\mathcal{S}$) [6–12], but also those at collider facilities (exploiting, typically $\mathcal{S}_1\mathcal{S}_2 \rightarrow \chi\chi\mathcal{S}_3$), whether it be the LHC [13], or low-energy facilities such as Belle [14–16] or DaΦNe [14]. Such non-observation tends to militate against the requirements for obtaining the correct relic-density, calling into question the entire paradigm. It should be realised, though, that event rates in such terrestrial experiments are governed by many assumptions about the nature of the interaction (*e.g.*, spin-dependence) or the identity of \mathcal{S} for the dominant process. For example, if \mathcal{S} were a third generation fermion, the signal rates would be quite suppressed, without unduly affecting cosmological evolution. Similarly, if χ were very heavy, not only would production at colliders be suppressed, but the consequent reduction in its number density (so as to maintain the requisite energy density) would also suppress the direct detection rates.

This, then brings us to the realm of indirect searches, nominally carried out through satellite-based and ground-based experiments [17–21]. The DM particles in open space can annihilate into a pair of SM particles and impinge on space-based detectors either directly, or at the end of a cascade of decays. Free from the aforementioned suppressions that often plague the other avenues, indirect searches proffer one of the most promising ways to not only detect the DM, but also to determine its properties. Signatures [19, 22, 23] include anomalous photon, positron or antiproton production that could be observed over and above known astrophysical sources.

In this paper, we concentrate on photon signals, which serve to provide some of the most robust and stringent constraints on DM annihilation into a variety of final states [24, 25]. Unlike charged particles, photons are not deflected by the presence of interstellar (or intergalactic) magnetic fields and thus we can trace them back to their origin with a high degree of confidence. Furthermore, the relatively small attenuation means that spectral properties of the source remain intact. As can be easily appreciated, the simplest and most unmistakable signal would be monochromatic photon emission resulting from either a two body final state (where the second particle need not be a photon) or from internal bremsstrahlung [26–30]. Of course, since the DM is electrically neutral¹, pair-annihilation into a two-body state with a photon can proceed only as a loop-level process. A second possibility exists, though, in the form of, say, $\chi\chi \rightarrow e^+e^-$ with the positron subsequently annihilating with a low-energy (and astrophysically produced) electron to lead to a nearly monochromatic photon line. In either

¹While millicharged DM can be accommodated in a specific class of models, we shall not consider such.

case, the effective cross section is small.

Much larger cross sections are obtained for processes that lead to a gamma-ray continuum (rather than a line emission) [31, 32]. These can, roughly, be divided into two classes, namely

- *prompt emissions* from dark matter annihilations into any SM pair $\mathcal{S}\bar{\mathcal{S}}$, with photon(s) being either radiated off or emanating from the decay of a particle that has arisen either directly from a primary decay product or as a result of its hadronization (such as $\pi^0 \rightarrow \gamma\gamma$). The photon energy could range from $E_{\max} (\lesssim M_\chi)$ all the way down.
- *secondary emissions* from the (quasi)stable, charged particles produced in the primary annihilation event. Inverse Compton scattering of relativistic particles with the cosmic microwave background radiation (CMBR) as well as starlight can give photons with energies in the X-ray band, whereas in the presence of astrophysical magnetic fields, synchrotron radiation (typically in the radio band) result.

Various astrophysical systems can be used to look for those aforementioned signal of DM. For example, the central region of ordinary Galaxies (like our own Milky Way or M31) are considered interesting arenas for WIMP searches [33–41]. Signals from these galactic central (GC) regions may also be used to understand the well known *cusp/core* issue of the innermost part of the DM distribution profile. However, photon signals of DM annihilation in the GC region can be contaminated by galactic diffuse emissions as well as electromagnetic radiations from various other nearby astrophysical object such as supernova remnants, pulsars etc. Owing to such unresolved backgrounds, GCs are not ideal for effecting precision studies [42–46].

N-body simulations indicate the existence of a large number of DM-dominated sub-halos around typical galaxies [47, 48]. Some of these sub-halos might be massive enough to host a dwarf galaxy [47], and these appear as dwarf spheroidal galaxies (dSphs). Constituting the largest galactic substructures around the Milky Way, these dSphs are expected harbour the densest DM distributions in the galactic halo, with a mass-to-light ratio lying in the range (100–1000) M_\odot/L_\odot , where M_\odot and L_\odot are the solar mass and the solar luminosity respectively. Their overwhelming DM content, minimal Galactic foreground emission, and lack of astrophysical radiation [49, 50] render the dSphs promising targets for the indirect detection of DM.

A decade after the Sloan Digital Sky Survey (SDSS) revealed a population of “ultrafaint” dwarf galaxies (UFDs) in the northern hemisphere (e.g., [51–53]), a new generation of sky surveys has begun charting the southern hemisphere. In the past few years, nearly two dozen UFDs have been discovered using data from Pan-STARRS ([54, 55]), the Dark Energy Survey ([56–59]), and other surveys using the Dark Energy Camera at Cerro Tololo ([60–63]).

Their small halo mass and negligible baryonic mass render UFDs extremely valuable laboratories for exploring the nature of dark matter. The southern UFDs provide new opportunities to address unanswered old questions about the nature and origin of Galactic substructure, and, in particular, the galactic luminosity function. While the latter continues to be revised, its faint end sets boundary conditions for galaxy formation within a given cosmological model ([64]). Due to their proximity, high dark-matter content, and the apparent absence of non-thermal processes, the Milky Way UFDs are excellent targets for the indirect detection of dark matter ([65, 66]).

We consider, here, electromagnetic radiation over a wide range, from gamma down to radio frequencies, emanating from UFDs. Surrounded by large-scale magnetic fields, the sheer size thereof confines the e^\pm produced by WIMP annihilation long enough for these to radiate substantially. Since the dSphs targeted by the space-based *Fermi* Large Area Telescope² (Fermi-LAT) have no millisecond pulsars associated with them [67], the astrophysical gamma-ray background is essentially negligible. Consequently, the non-observation of such high energy gamma-rays or radio-emission from nearby dSphs may be used to put strong constraints on the dark matter annihilation/decay rates. To this end, we consider fourteen recently discovered UFDs and analyse nearly eleven years of gamma-ray data collected by the Fermi-LAT Collaboration. Amongst them, 13 UFDs are Milky Way satellites and one (Eridanus II) is from the Local field (LF) (Local Field dwarf spheroidal galaxies are not bound to Milky Way and M31). We also include the classical dSph Draco in our analysis which has been extensively considered in the literature for indirect detection of DM [32, 68, 69].

The remaining of the paper is organized as follows: in Section 2, we describe the different components of the γ -ray flux and the astrophysical J -factor for the different dSphs. This is followed, in Section 2.2, by a discussion of different possible dark matter profiles, and the consequent J -factors. In Section 3, we analyze the Fermi-LAT data for different dwarf spheroidal galaxies to obtain upper limits on the annihilation cross sections for different channels. We also examine the uncertainty accruing from the determination of astrophysical parameters and the choice of the dark matter profile. In Section 4, we focus on the synchrotron radiation from the dwarf spheroidal galaxies, especially in the context of the existent radio telescopes such as from Giant Metrewave Radio Telescope (GMRT) and Very Large Array (VLA) telescope and the projected sensitivity of the Square Kilometer Array (SKA). This is followed, in Section 5, by an examination of the role of astrophysical uncertainties in the determination of the constraints. And, finally we conclude, in Section 6, along with a discussion of the relative strengths of various observations and possible future developments.

²<http://fermi.gsfc.nasa.gov>

2 γ -ray flux from pair-annihilation of WIMPs

A given scenario may include multiple new WIMP candidates (\mathcal{W}_i), of which perhaps only one could constitute the DM. Indirect detection of the said WIMPs depends on two key processes : (i) the pair annihilation of the WIMPs through processes such as $\mathcal{W}_i\mathcal{W}_j \rightarrow \sum_k \mathcal{S}_k$, or (ii) the decay³ of a WIMP into SM particles, namely $\mathcal{W}_i \rightarrow \sum_k \mathcal{S}_k$. In each case, a bunch of energetic standard model particles result in the final state, either directly from the aforementioned processes or as a result of the subsequent decay cascades of the \mathcal{S}_k . However, it should be noted that neither of the two processes are a must in a given particle dark matter scenario. Furthermore, they bear relevance (apart from in the cosmological context) only if they occur at a rate that can be detected on various experimental facilities based on the earth or on satellites. This relevance is, of course, determined jointly by their rates and the detectability (in terms of the final particle identities and the energies they carry), in such facilities, earth-bound or satellite-based [71–79]. These, in turn, are determined by the details of the underlying particle physics model, both in terms of the spectrum as well the sizes, or even the existence, of the couplings. In addition to these, several astrophysical input parameters also play a major role in the final observation (both in the annihilation rate as well as in the propagation of various standard model particles through the space). Some of these astrophysical parameters, understandably, contain large uncertainties rendering any conclusive prediction of the indirect signature of the dark matter very challenging[80].

In this analysis, we focus on the annihilation of Majorana dark matter in an almost model independent manner, with the simplifying assumption that the pair-annihilation proceeds into a single channel alone, with a 100% probability. The consequent individual sensitivities/constraints can, then, be convoluted, in a relatively straightforward manner, to that applicable for a given realistic model. The DM annihilation rate per unit volume is given by $\langle\sigma v\rangle\rho_\chi^2/2M_\chi^2$, where ρ_χ is the density, σ the cross section and v the velocity of the second DM particle in the rest frame of the first⁴. The thermal average $\langle\sigma v\rangle$ is estimated using the knowledge of particle physics and is model-specific. On the other hand, assuming that the DM density has a spherical symmetry (a very good approximation), the radial dependence of ρ_χ is modelled based on astrophysical observations, as we shall discuss later. For a specific energy $E(\equiv E_\gamma)$, the differential γ -ray flux $\phi_{\text{WIMP}}(E, \Delta\Omega)$ (in units of photons $\text{cm}^{-2}\text{s}^{-1}\text{GeV}^{-1}$) lying within a solid angle $\Delta\Omega$ and having arisen from the annihilations of WIMPs of mass M_χ , can

³In the second case, clearly \mathcal{W}_i is not protected by a discrete symmetry. It could have arisen, for example, from the pair-annihilation of a Z_2 -odd DM, namely $\chi\chi \rightarrow \mathcal{W}_i\mathcal{W}_j$. It should be realised though that a decaying DM is also admissible as long as the decay is very slow, as, for example, happens in gravity-mediated decays [70].

⁴For a DM annihilation rate of $\langle\sigma v\rangle \sim 10^{-26} \text{ cm}^3/\text{s}$ —one that is consistent with the correct relic density for $M_\chi \sim \mathcal{O}(10^{2-3}) \text{ GeV}$ —an observable flux of gamma rays is obtained.

be expressed [81] as a product of two terms, one each accounting for the particle-physics and astrophysics factors, namely

$$\phi_{\text{WIMP}}(E, \Delta\Omega) = \Phi^{pp}(E) \times J(\Delta\Omega) . \quad (2.1)$$

The particle physics factor can be written as [81]:

$$\Phi^{pp}(E) = \frac{\langle\sigma v\rangle}{8\pi M_\chi^2} \sum_f \frac{dN_{\gamma,f}}{dE} B_f , \quad (2.2)$$

where $dN_{\gamma,f}/dE$ is the differential photon spectrum (per annihilation event) for a given final state 'f', and B_f is the corresponding branching fraction. Several numerical packages like Pythia [82], DarkSUSY ([83]), DMFit [84] etc. are designed to estimate differential photons yields from each annihilation channel. While the selection of standard model final states, through which annihilation would occur (e.g. $b\bar{b}$, $\tau^+\tau^-$, $\mu^+\mu^-$ etc.), is theoretically motivated, as stated above, we remain agnostic and consider only a single channel dominance. Thus, unless otherwise mentioned, in the rest of the analysis, only a single final state ($b\bar{b}$, $\tau^+\tau^-$, $\mu^+\mu^-$) will be considered to have been produced (*i.e.*, with 100% probability) in a DM annihilation process, and consequent limits obtained on the cross sections.

2.1 Astrophysical Factor (J)

Since the total flux is proportional to the factor J , it behaves us to examine it closely. As we are primarily concerned with pair annihilations, it should depend on ρ_χ^2 . While the galactic center, where ρ_χ is the largest, is associated with the highest flux, it is also associated with an intense astrophysical background. In contrast, the UFDs present features that make them ideal sources. The typical values of the J -factor [85] for the GC are $J \approx 10^{22} - 10^{23} \text{GeV}^2 \text{cm}^{-5}$, while $J \approx 10^{16} - 10^{19} \text{GeV}^2 \text{cm}^{-5}$ for UFDs and $J \approx 10^{15} - 10^{19} \text{GeV}^2 \text{cm}^{-5}$ for galaxy clusters.

While the aforementioned quadratic dependence is indicative, a true measure of the effective J involves the line-of-sight (l.o.s) integration of the same, namely [81]

$$J(\Delta\Omega) = \int \int \rho_\chi^2(r(\lambda)) d\lambda d\Omega = 2\pi \int_{\theta_{\min}}^{\theta_{\max}} d\theta \sin\theta \int_{\lambda_{\min}}^{\lambda_{\max}} d\lambda \rho_\chi^2(r(\lambda)) , \quad (2.3)$$

where λ is the l.o.s distance and θ is the angle between the l.o.s and the center of the UFD. The galactocentric distance $r(\lambda)$ is obtained in terms of the UFD's distance d from the Sun through

$$r(\lambda) = \sqrt{\lambda^2 + d^2 - 2 \lambda d \cos\theta} . \quad (2.4)$$

The DM density profile in UFDs remain a topic of debate. Two broad classes are popularly used to fit the observational data, namely those with a cusp-like profile[86] or a cored profile[87–89] respectively. While the lack of sufficient kinematical observational

prevents the selection of a particular profile type, N-body cosmological simulations, with the most recent results, favors the cuspy Navarro-Frenk-White (NFW) form [86], specially for dSphs and UFD galaxies. This is parameterized as [86]

$$\rho_\chi(r) = \frac{\rho_s r_s^3}{r(r_s + r)^2}, \quad (2.5)$$

where ρ_s and r_s are the characteristic density and scale radius respectively. These, as well as another one, namely, r_h (that we would find useful when we discuss synchrotron radiation in Sec.4) can be obtained using d , θ_{max}^0 , $\sigma_{l.o.s}$ and $r_{1/2}$. Here d , $r_{1/2}$ and $\sigma_{l.o.s}$ denote the heliocentric distance, the half-light radius and the velocity dispersion of each UFD galaxy. θ_{max}^o is the angle made by the outer most star of the UFD. While the details can be found in ref.[90], we discuss the relations briefly.

To begin with, consider the mass $M_{1/2}$ contained within the half-light radius ($r_{1/2}$) of the UFD and approximately expressed in terms of $r_{1/2}$ and the UFD velocity dispersion $\sigma_{l.o.s}$ as

$$M_{1/2} = M(r_{1/2}) \approx \frac{2.5}{G_N} \sigma_{l.o.s}^2 r_{1/2}. \quad (2.6)$$

where G_N is Newton's constant. The NFW parameter r_s can be approximated in terms of $r_{1/2}$, *viz.*

$$r_s = 5 r_{1/2}, \quad (2.7)$$

whereas ρ_s is given by

$$\rho_s = \frac{M_{1/2}}{4\pi r_s^3} \left[\log \left(\frac{r_s + r_{1/2}}{r_s} \right) - \frac{r_{1/2}}{r_s + r_{1/2}} \right]^{-1}. \quad (2.8)$$

The distance to the outermost star of the UFD from the center of UFD is, of course,

$$r_{\max} = d \sin \theta_{\max}^o. \quad (2.9)$$

The definition of the diffusion radius (r_h) is somewhat ambiguous, and depends on the spatial extent of both the gas and the magnetic field, quantities that are poorly understood for dSphs. One could draw inspiration from the Milky Way where the height of the diffusion cylinder is a few times the size of the stellar disc width. Given that this is the typical extent of the interstellar gas for galaxies, we assume [32, 91] that

$$r_h \approx 2 r_{\max} = 2 d \sin \theta_{\max}^o. \quad (2.10)$$

We have checked that varying r_h by a factor 0.5–2 does not alter the results to a great extent.

Using eqns.(2.8–2.10) with the values of the parameters d , $\sigma_{l.o.s}$, and $r_{1/2}$ given in Table A–I of the Appendix, we calculate the parameters ρ_s , r_s and r_h and list them in Table 1.

dSphs	d(Kpc)	$r_h(Kpc)$	$\rho_s(GeV/cm^3)$	$r_s(Kpc)$
Aquarius II	107.9	0.42	2.27	0.615
Carina II	37.4	0.3	1.78	0.38
Draco II	20	0.07	71.73	0.06
Eridanus II	366	0.792	1.454	0.88
Grus I	120.2	0.39	6.7	0.26
Horologium I	79	0.188	30.55	0.16
Hydra II	151	0.448	< 8.24	0.335
Leo V	173	0.465	23.83	0.15
Pegasus III	215	0.228	40.73	0.185
Pisces II	183	0.438	8.93	0.24
Reticulum II	30	0.251	10.08	0.16
Tucana II	57.5	0.452	3.6	0.575
Tucana III	25	0.174	< 2.29	0.215
Triangulum II	30	0.157	< 46.1	0.14
Draco	80	2.5	1.4	1.0

Table 1: *The values of the astrophysical parameters for the 13 newly discovered UFDs [92] and the classical dSph Draco. The parameters for the 13 UFDs in this table correspond to the central values of the parameters in Table A–I. The parameters for Draco has been taken from [93].*

The parameters in Table 1 correspond to the central values of the parameters in Table A–I of the appendix.

Given the measurements of ρ_s and r_s , it is a straightforward task to determine J . In Table 2, we present this for a set of UFDs, adopting, in each case, the standard choices of $\theta_{\min} = 0$ and $\theta_{\max} = 0.5^\circ$. While the point spread function (PSF) of the Fermi-LAT varies with the energy of the incident photons, for the energy range of our interest in the Fermi-LAT analysis, the average PSF value of the LAT detector roughly equals 0.5° [19, 72, 94, 95].

The calculation of J for a dSph is beset with several uncertainties. The relative paucity of identifiable stars in such galaxies renders spectroscopic studies difficult. The small sample size, for one, results in significant statistical errors. Moreover, the lack of sufficiently large stellar kinematic data from the spectroscopic observations results in large systematic uncertainties in the determination of the velocity dispersions and, therefore, the mass [66, 92]. To handle this, we use an algorithm developed by some of us [96], using Monte Carlo methods and distributions of the variables d , $\sigma_{1.o.s}$ and $r_{1/2}$. The asymmetrical error bars (including

systematics) are modelled by skew normal distributions with unequal values for the standard deviation on each side of the mean. The resultant uncertainties in the J -factor are displayed in Table 2.

For comparison, we also list the corresponding values derived by Pace *et al.* [92], using an empirical scaling relation motivated by the analytical work of Evans *et al.* [90]. For the NFW profile, the empirical relation reads

$$\frac{J(0.5^\circ)}{\text{GeV}^2\text{cm}^{-5}} \approx 10^{17.72} \left(\frac{\sigma_{\text{l.o.s}}}{5 \text{ km s}^{-1}} \right)^4 \left(\frac{d}{100 \text{ kpc}} \right)^{-2} \left(\frac{r_{1/2}}{100 \text{ pc}} \right)^{-1}, \quad (2.11)$$

It is worth pointing out the remarkably good agreement between the exact numerical result and the empirical formula. Indeed, at the level of accuracy of our results, the two are virtually indistinguishable. Nonetheless, we use the exact results (as derived using 2.3 along with the data listed in the Appendices) for our subsequent numerical calculations. It should be borne in mind, though, that a different choice of the density profile would lead to a substantially different value for J , a point that we would return to at a later section. It should also be noticed that, for certain UFDs, only upper bounds on the J -factor exists. This can be traced to the insufficiency of the kinematic data, which leads to only an upper bound on the velocity dispersion and, hence, on the J -factor [79].

2.2 Dependence of J on the density profiles

While the NFW is a traditional benchmark choice for the DM profile motivated by the N -body simulations, its cusp-like nature at the center of the galaxy is quite different from the alternate cored profiles. While we would use the NFW for most of our numerical results, it is an imperative to ensure that the cuspy nature does not lead to extreme answers, To this end, we examine two examples of the second category, namely the pseudo-isothermal(ISO) [89] profile and the one originally proposed by Burkert [87, 88]. These are given by

$$\rho_{\text{ISO}}(r) = \frac{\rho_c r_c^2}{r^2 + r_c^2}, \quad \rho_{\text{Burkert}}(r) = \frac{\rho_B r_B^3}{(r_B + r)(r_B^2 + r^2)} \quad (2.12)$$

where r_B and r_c represent the respective core radii, whereas ρ_c and ρ_B are the corresponding densities at the very center. While $\rho_{\text{Burkert}}(r)$ resembles an isothermal profile in the inner regions ($r \ll r_B$), for large r it falls off much faster (r^{-3} versus r^{-2}). As in the case for the NFW profile, the parameters are to be determined from observational data related to a given galaxy. While the density profiles are undoubtedly different, having been deduced from the same data, they ought to generate virtually identical galactic rotation curves. Demanding this, ref.[97] deduced approximate relations between the parameters for the three profiles, *viz.*, $r_s \simeq 6.1r_c \simeq 1.6r_B$ and $\rho_s \simeq 0.11\rho_c \simeq 0.37\rho_B$. With such choices, the consequent rotation

Galaxy	$\log_{10}(J/\text{GeV}^2 \text{ cm}^{-5})$			
	Pace <i>et al</i> [92] (NFW)	Direct Integration		
		NFW	Burkert	ISO
Aquarius II	$18.27^{+0.66}_{-0.58}$	$18.11^{+0.68}_{-0.63}$	$18.53^{+0.72}_{-0.66}$	$18.01^{+0.73}_{-0.66}$
Carina II	$18.25^{+0.55}_{-0.54}$	$18.16^{+0.55}_{-0.53}$	$18.45^{+0.60}_{-0.56}$	$18.05^{+0.58}_{-0.54}$
Draco II	$18.93^{+1.39}_{-1.70}$	$19.07^{+1.33}_{-1.69}$	$19.54^{+1.35}_{-1.70}$	$18.90^{+1.34}_{-1.70}$
Eridanus II	$17.28^{+0.34}_{-0.31}$	$17.14^{+0.35}_{-0.30}$	$17.68^{+0.35}_{-0.31}$	$17.06^{+0.35}_{-0.31}$
Grus I	$16.88^{+1.51}_{-1.66}$	$16.94^{+1.57}_{-1.74}$	$17.48^{+1.60}_{-1.75}$	$16.76^{+1.54}_{-1.67}$
Horologium I	$19.27^{+0.77}_{-0.71}$	$19.01^{+0.83}_{-0.73}$	$19.37^{+0.85}_{-0.75}$	$18.73^{+0.85}_{-0.75}$
Hydra II	< 17.77	< 17.92	< 18.46	< 17.84
Leo V	$17.65^{+0.91}_{-1.03}$	$17.91^{+1.03}_{-1.06}$	$18.51^{+1.02}_{-1.08}$	$17.84^{+1.01}_{-1.07}$
Pegasus III	$18.30^{+0.89}_{-0.97}$	$18.46^{+0.94}_{-1.05}$	$19.06^{+1.02}_{-1.07}$	$18.39^{+1.03}_{-1.05}$
Pisces II	$17.30^{+1.00}_{-1.09}$	$17.53^{+1.02}_{-1.09}$	$18.10^{+1.04}_{-1.09}$	$17.45^{+1.03}_{-1.09}$
Reticulum II	$18.96^{+0.38}_{-0.37}$	$18.76^{+0.43}_{-0.42}$	$19.21^{+0.43}_{-0.42}$	$18.66^{+0.43}_{-0.42}$
Triangulum II	< 19.73	< 19.74	< 20.18	< 19.64
Tucana II	$19.02^{+0.58}_{-0.53}$	$18.93^{+0.62}_{-0.58}$	$19.22^{+0.64}_{-0.61}$	$18.83^{+0.66}_{-0.62}$
Tucana III	< 17.71	< 17.87	< 18.20	< 17.76
Draco	$18.83^{+0.12}_{-0.12}$	$18.85^{+0.12}_{-0.12}$	$19.08^{+0.13}_{-0.13}$	$18.75^{+0.13}_{-0.13}$

Table 2: The J -factors for the various UFDs as obtained by directly integrating eqn. 2.3 for three density profiles and for $\theta_{max} = 0.5^\circ$. Also shown, for comparison, are the values obtained by Pace *et al.* [92], for the NFW profile, using an approximate scaling relation.

curves were found to be virtually indistinguishable for $r \lesssim 2r_s \simeq 12r_c$, *i.e.*, almost the entire observed range.

While N -body simulations [98, 99] tend to favour a cuspy profile (such as the NFW) over the smooth (and relatively flat at the center) profiles such as the Burkert or the ISO, insufficient kinematic data (such as those on rotational curves) prevent us from strongly favoring any one profile. Indeed, some observations [100] actually favour cored halos over cuspy ones. Fortunately for us, the J -factor does not have too strong a dependence on the choice. Indeed, as Table 2 demonstrates, the NFW profile leads to values that are not too far from the average of those obtained from the three profiles. In other words, the theoretically favoured choice is also a good representative.

3 Analysis of γ -ray fluxes from ultra-faint dwarf galaxies

Several features of gamma rays make them an ideal medium for indirect DM detection. Unlike the charged particles, these do not get deflected by the presence of strong magnetic fields and thus we can trace back the origin of the emission. In addition, gamma rays suffer very little attenuation and hence the spectral properties of the source remain intact. In studying γ -rays originating from pair annihilations of DM into SM particles within UFDs, we consider the data from the Large Area Telescope (LAT) on board the Fermi observatory. The Fermi-LAT is a γ -ray pair conversion space-based detector that scans the whole sky every 3 hours from a low-Earth orbit of 565 km altitude at a 25.6-degree inclination with an eccentricity < 0.01 . Launched on June 11, 2008, by the Delta II Heavy launch vehicle from Cape Canaveral, the principal objective of the Fermi-LAT was to conduct a long term high sensitivity γ -ray observations of celestial sources in the energy range from ≈ 20 MeV to > 500 GeV [101] and we analyze over ten years (2008-09-01 to 2019-02-04) worth of this sky survey data. While several dwarf spheroidals have been observed over the past few years, no conclusive signal has been found from any of them. Given that such negative results too can provide important information about the dark matter [19, 94, 95, 102, 103], we study a set of 14 UFDs which have been recently discovered in several surveys (see Appendix A for a list). Using the latest version of Fermi ScienceTools (v1.2.1) for our analysis, we process the data with an improved PASS 8 instrument response function (IRF), in particular the source class IRF, P8R3_SOURCE_V2. Furthermore, the tool ‘*gtmktime*’ has been used to extract the “good time interval” data from the whole data set. Extracting the LAT data within a 15° radius of interest (ROI) around each source, we consider only a limited range for the reconstructed energy E , *viz.* $E \in [0.1, 300]$ GeV, so as to reduce possible uncertainties at low energies on the one hand and background contamination at high energies on the other. To remove the possible contamination from the earth albedo, we apply a zenith-angle cut at 90° as recommended by the Fermi-LAT analysis team. With the Earth’s limb lying at a zenith angle of 113° , the application of a zenith cut at 90° eliminates a large fraction of the background atmospheric gamma-rays.

The binned likelihood analysis for the extracted data set was performed with the ‘*gtlike*’ tool [104, 105]. To this end, we first generate a source model file with the inclusion of all the sources from the 4FGL catalog [106] within a 20° ROI from the position of the ‘source of interest’. Note that we extend the spatial coverage up to 20° ROI to account for possible overlapping between the point spread functions of nearby sources. In addition, to eliminate possible background effects resulting from galactic and extra galactic diffuse emission, we add the Galactic diffuse model (*gll_iem_v07.fits*) and the isotropic extra galactic diffuse model (*iso_P8R3_SOURCE_V2_v1.txt*) to the source model. The spectral parameters of

all the 4FGL sources [106] within ROI, as well as the normalization parameters of two diffuse models have been left free in the fitting procedure. The rest of the background sources within the $20^\circ \times 20^\circ$ ROI have been kept fixed at their values given in the 4FGL catalog [106]. Table A-II, in the Appendix, lists all the parameters used at different stages of the analysis of the data.

3.1 Constraints on DM annihilation with eleven years of Fermi-LAT data

To search for γ -ray emissions coincident with our targets, we first model our sources with a power-law spectral model ($dN/dE \propto E^{-\Gamma}$) with spectral index $\Gamma = 2$ [19, 79, 94, 95]. As a statistical discriminator, we use the ratio of the maximum likelihoods for two hypotheses, namely, $TS = -2 \ln \left(L_{(\max,0)} / L_{(\max,1)} \right)$, where $L_{(\max,1)}$ and $L_{(\max,0)}$ respectively denote the maximum likelihood in the presence of a signal and the null hypothesis. In other words, a value $TS > 25$ would correspond to a “ 5σ discovery”.

UFD	$TS_{\text{peak}}(b)$	$TS_{\text{peak}}(\tau)$
Aquarius II	2.88	2.94
Carina II	1.24	1.81
Draco II	1.37	1.88
Eridanus II	0.81	1.23
Grus I	1.59	1.65
Horologium I	4.21	4.71
Hydra II	2.21	2.31
Leo V	0.88	0.92
Pegasus III	1.91	2.13
Pisces II	1.22	1.96
Reticulum II	4.85	4.95
Tucana II	11.87	12.47
Tucana III	4.36	4.53
Triangulum II	1.19	1.25

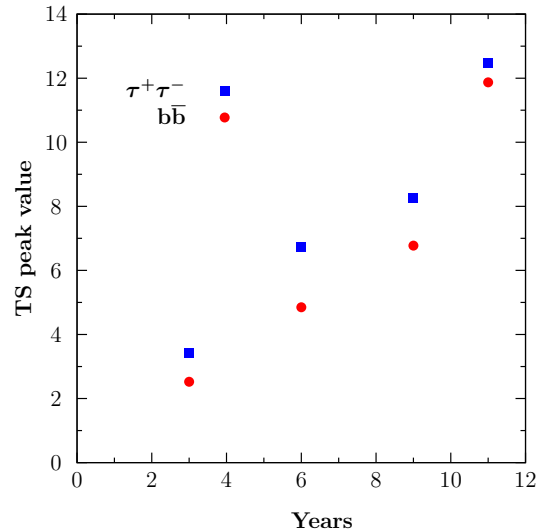


Figure 1: The TS peak value for two annihilation final states as evinced by the Fermi-LAT data (left panel). The change in the TS value for Tucana II, as a function of telescope operation time, for excess γ -ray emission from the direction of Tucana II (right panel).

Unfortunately, as Fig.1(a) attests, except for Tucana II, the other target UFDs have not yet shown any faint emission from their location (i.e. $TS \lesssim 5$). And while an intriguing hint of a faint gamma-ray signal has been reported [79], from the direction of Tucana II, the excess is still too small to claim a real discovery. Quite hearteningly, though, the significance of the putative excess has only grown with more data, as is evinced by Fig.1(b), thereby raising hope that a signal may yet be established.

Meanwhile, in the absence of a discernible signal from an UFD can be used to impose 95% C.L. upper limits on the γ -ray flux from the site. In this, we use the Bayesian approach [107]—already implemented in the `pyLikelihood` module of `ScienceTools`—as this is more sensitive [108, 109] than the profile likelihood method for low statistics.

These limits are displayed in Fig. 2. Naively, one might expect that such upper limits on the flux should be independent of the mass of the DM or the channel it annihilates into. We need to appreciate though that the γ -ray spectrum is strongly dependent on each of these factors. Various factors contribute to this. These include the charge and mass of the radiating particle as well as whether cascade decay play a major role. And since the detector acceptances and efficiencies (not to speak of the galactic backgrounds) have strong energy-dependence, it stands to reason that the limits thus derived would also do so. This is reflected by Fig. 2. It is interesting to note that, for the most of range of M_χ considered here, the strongest limits are obtained for the classical dwarf Draco. However, much of this is due to astrophysical factors, and as we shall soon see, this does not imply that the best bounds on the annihilation rate would be associated with Draco.

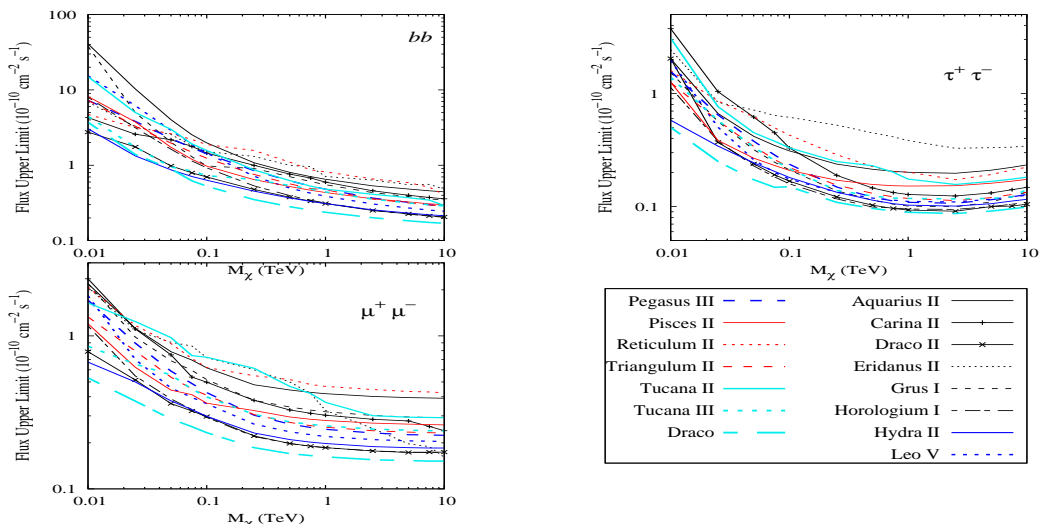


Figure 2: 95% C.L. upper limits on the γ -ray fluxes (from DM pair-annihilations in UFDs) as a function of M_χ . In deriving these, the indicated channel is assumed to be an exclusive one.

Such upper limits on the γ -ray fluxes from DM annihilation can be translated to constraints in the two dimensional plane of the WIMP mass (M_χ) and the thermally averaged pair-annihilation cross section ($\langle\sigma v\rangle$). This exercise, though, depends on the final states resulting from the annihilation processes and, hence, on the details of the model. However, as indicated at the outset, we adopt an agnostic standpoint and consider three *exclusive* channels, namely $b\bar{b}$, $\tau^+\tau^-$ and $\mu^+\mu^-$. To estimate the limits on $\langle\sigma v\rangle$, we fit the γ -ray spectrum

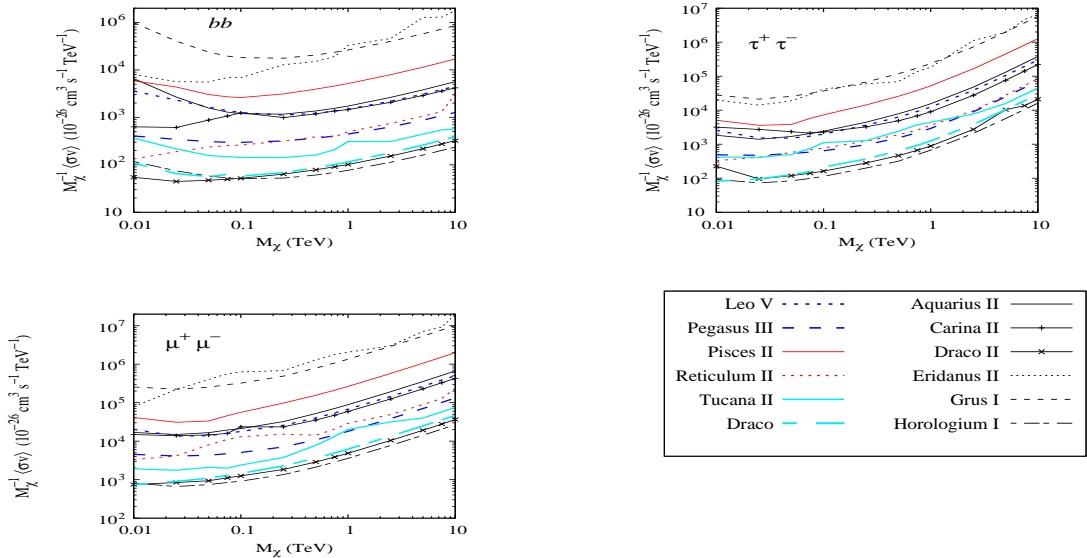


Figure 3: 95% C.L. upper limit on the thermally averaged WIMP pair-annihilation $\langle\sigma v\rangle$ as derived from the upper limits on the gamma-ray fluxes from individual UFDs. In each case, the annihilation channel is assumed to be exclusive. (No limits result from Hydra II, Triangulum II and Tucana III as there exist only upper limits on the corresponding J -factors.).

arising from the DM-dominated UFDs with an MC-simulated DM self-annihilation spectrum, DMFitFunction⁵ [84]. The DMFit package is based on the particular set of MC simulations of hadronization and/or decay of the annihilation products as used by the DarkSUSY [83] team.

The consequent limits, for individual UFDs, are displayed in Fig. 3 for each of the three annihilation channels. The limits thus obtained are strongly dependent on various astrophysical parameters that enter in the calculation through the J -factor and the dark matter density profile (see eqns.(1) & (2)). These parameters vary substantially between different UFDs and, as a result, Horologium I, due to its J -factor being the largest, provides the strongest limits on $\langle\sigma v\rangle$ for all three DM annihilation channels. However, one should keep in mind that among the newly found UFDs, Horologium I is plagued with large uncertainties in its J -value compared with the classical dwarf Draco. Thus the obtained limit from it may not be as robust as the one from Draco. In section 5.1, we provide a detailed discussion on the J -factor uncertainties for Horologium I and Tucana II.

⁵https://fermi.gsfc.nasa.gov/ssc/data/analysis/scitools/source_models.html

3.2 Comparison between our obtained result from the Fermi-LAT analysis with the estimated limits provided by Planck

Several disparate cosmological observables can probe the DM sector. In the early epoch of the universe, WIMP annihilation could inject electromagnetic radiation as well as energetic particles into the plasma thereby altering the fine-grained evolution. Of the myriad such effects, two particular ones, namely those pertaining to Big Bang Nucleosynthesis (BBN) and the Cosmic Microwave Background (CMB) are important in our context (with others like primordial black hole formation or HI line strengths *etc.* playing only subservient roles. The injection of high energy particles (hadrons) and radiation during or after BBN can modify light nuclei abundances, thus coming into conflict with the data. The limits, understandably, depend on both the mass of the DM and the annihilation channel. For $M_\chi \sim 1$ TeV, typical limits range over $\langle\sigma v\rangle \sim 10^{-23} - 10^{-21}$ cm³/sec [110], depending on the details of the annihilation mechanism and the consequent effect on the particular light element being synthesised. Evidently, the BBN limit is a few orders of magnitude higher than the thermal cross-section and, thus, do not pose any threat to such heavy WIMPs.

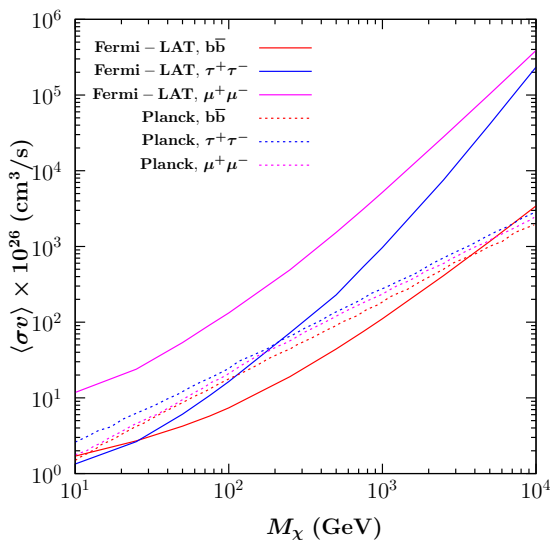


Figure 4: Comparison between the limits obtained for Horologium I from Fermi-LAT with the limits provided by Planck.

On the other hand, the injection of such charged particles could significantly increase the residual ionization fraction which, in turn, modifies the last scattering surface as well the observed CMB anisotropy [111, 112]. The WMAP [113] and, more recently, the Planck [114] satellite experiments are highly sensitive to any such modifications in the CMB, leading to

strong and model-independent limits on the aforementioned energy-injections [114]. These limits can, further, be translated into constraints on WIMP annihilation cross sections. As the Horologium I provided the strongest limits on γ -ray fluxes as seen by Fermi-LAT, in Fig. 4, we compare the same with the constraints from Planck data. It is clear that, for the $b\bar{b}$ channel, the Fermi-LAT limits are stronger than the Planck limits over the entire range $M_\chi \in [10, 10^4]$ GeV, with the CMB constraints like to dominate only for $M_\chi \gtrsim 20$ TeV. For the $\mu^+\mu^-$ channel, the situation is quite the opposite, with the Planck measurement providing the most stringent limits. And, finally, the situation for the $\tau^+\tau^-$ channel is halfway in between with the Fermi-LAT constraints being stronger for $M_\chi \lesssim 500$ GeV and the Planck limits being dominant for larger masses. This puts into perspective the fact that a comprehensive probe of the DM parameter space is best achieved by a combination of search strategies, an issue we return to later.

4 Synchrotron radiation from ultra-faint dwarf galaxies

A charged particle propagating through the interstellar medium would lose energy owing to a variety of electromagnetic processes such as inverse Compton radiation, synchrotron radiation, Coulomb losses and bremsstrahlung. While this applies to any charged particle, the radiation would be substantial only if the particle is sufficiently long-lived, or in other words if it is one of e^\pm or p, \bar{p} . The contributions from the last two are much smaller, both on account of their larger masses as well as the small probability for a quark (from the hard process) fragmenting⁶ into a p, \bar{p} . Given this, we develop the subsequent arguments for e^\pm alone. The other species can be treated analogously.

A complete treatment of the DM-initiated synchrotron radiation must consider the diffusion of the secondary particles, and the aforementioned energy loss contributions therefrom. The formalism, developed in refs.[31, 32, 93], can be summarised by the transport equation for $n_e(\mathbf{r}, E)$, the number density of e^\pm of a given energy E at the position \mathbf{r} with respect to the center of the UFD), *viz.*,

$$\frac{\partial}{\partial t} \frac{dn_e(\mathbf{r}, E)}{dE} = \nabla \cdot \left(D(E, \mathbf{r}) \nabla \frac{dn_e(\mathbf{r}, E)}{dE} \right) + \frac{\partial}{\partial E} \left(b(E, \mathbf{r}) \frac{dn_e(\mathbf{r}, E)}{dE} \right) + Q_e(E, \mathbf{r}). \quad (4.1)$$

Here, $D(E, \mathbf{r})$ is the space-dependent diffusion coefficient, $b(E, \mathbf{r})$ encapsulates the energy loss term and the source term Q_e is given by

$$Q_e(E, \mathbf{r}) = \frac{\rho_\chi^2(\mathbf{r}) \langle \sigma v \rangle}{2m_\chi^2} \frac{dN_e}{dE}, \quad (4.2)$$

⁶Similarly, the probability for a charged particle to traverse unmolested from the UFD to the earth- or satellite-bound detectors is rather low. Consequently, the corresponding bounds from antiproton or positron detection are much weaker.

where N_e is the number of e^\pm produced with a given energy E per DM annihilation.

The energy loss term consists of several independent contributions from the processes listed earlier and is given by [31, 93]

$$\begin{aligned} b(E) &= b_{\text{IC}}(E) + b_{\text{syn}}(E) + b_{\text{Coul}}(E) + b_{\text{brem}}(E) \\ &= b_{\text{IC}}^0 E^2 + b_{\text{syn}}^0 B^2 E^2 + b_{\text{Coul}}^0 n(1 + \log(\gamma/n)/75) + b_{\text{brem}}^0 n(\log(\gamma/n) + 0.36). \end{aligned} \quad (4.3)$$

where the dependence on \mathbf{r} has been suppressed. Here, B is the magnetic field in μG , n is the number density of thermal electrons in cm^{-3} and $\gamma = E/m_e$ is the time-dilation factor. The various energy loss parameters b_{IC}^0 , b_{syn}^0 , b_{Coul}^0 and b_{brem}^0 have approximate values of 0.25, 0.0254, 6.13 and 1.51 respectively in units of $10^{-16} \text{ GeV s}^{-1}$ [31]. A position-dependence in $D(E, \mathbf{r})$ would be expected to be occasioned only by deviations from a homogeneous mass distribution. Given the low light-to-mass ratio for the UFDs, this is not expected to be a major concern. In the absence of a detailed knowledge of the structure of the UFDs, we neglect such dependencies, limiting ourselves to $D(E, \mathbf{r}) = D(E)$ with [93, 115]

$$D(E) = D_0 \left(\frac{E}{1 \text{ GeV}} \right)^{\gamma_D}. \quad (4.4)$$

Assuming spherical symmetry, a uniform magnetic field and a uniform number density of thermal electrons, the stationary state solution of the diffusion equation is given by

$$\frac{dn_e}{dE}(r, E) = \frac{1}{b(E)} \int_E^{M_\chi} dE' G(r, v(E) - v(E')) Q_e(E', r), \quad (4.5)$$

where the Green's function is given by

$$\begin{aligned} G(r, \Delta v) &= \frac{1}{\sqrt{4\pi\Delta v}} \sum_{k=-\infty}^{\infty} (-1)^k \int_0^{r_h} dr' \frac{r'}{r_k} \left(\frac{\rho_\chi(r')}{\rho_\chi(r)} \right)^2 \\ &\quad \left[\exp\left(-\frac{(r' - r_k)^2}{4\Delta v}\right) - \exp\left(-\frac{(r' + r_k)^2}{4\Delta v}\right) \right], \end{aligned} \quad (4.6)$$

with

$$v(E) \equiv \int_E^{M_\chi} d\tilde{E} \frac{D(\tilde{E})}{b(\tilde{E})}, \quad r_k \equiv (-1)^k r + 2kr_h. \quad (4.7)$$

Here r_h defines the diffusion zone of the UFD, namely the radius at which the free escape boundary condition $dn_e(r_h, E)/dE = 0$ may be imposed. Typically, r_h is approximately twice the radius of the last stellar component of the galaxy (*i.e.*, twice the distance of the outermost star from center).

The synchrotron power spectrum or the total power radiated per unit frequency at ν by an electron of energy E present in a magnetic field B , *viz.*, $P_{\text{synch}}(\nu, E, B)$ is defined as:

$$P_{\text{synch}}(\nu, E, B) = \pi\sqrt{3}r_0 m_e c \nu_0 \int_0^\pi d\theta \sin^2 \theta F\left(\frac{x}{\sin \theta}\right), \quad (4.8)$$

where θ is the pitch angle, $r_0 = e^2/(m_e c^2)$ is the classical electron radius and $\nu_0 = eB/(2\pi m_e c)$ is the non-relativistic gyro-frequency. While

$$F(y) = y \int_y^\infty d\zeta K_{5/3}(\zeta) \simeq 1.25 y^{1/3} e^{-y} (648 + y^2)^{1/12}, \quad (4.9)$$

the quantity x is given by

$$x = \frac{2\nu m_e^2 (1+z)}{3\nu_0 E^2} \quad (4.10)$$

with z being the redshift of the source. For the UFDs under consideration, $z \approx 0$.

We can, now, estimate the total energy radiated or the local emissivity (i.e. the amount of energy radiated at a given r , per unit volume per unit time) at a given frequency ν in the form of synchrotron radiation in terms of P_{synch} and dn_e/dE viz.,

$$j_{\text{synch}}(\nu, r) = \int_{m_e}^{M_x} dE \left(\frac{dn_{e^+}}{dE} + \frac{dn_{e^-}}{dE} \right) P_{\text{synch}}(\nu, E, B) = 2 \int_{m_e}^{M_x} dE \frac{dn_{e^-}}{dE} P_{\text{synch}}(\nu, E, B). \quad (4.11)$$

The integrated synchrotron flux density spectrum is, now, given by

$$S_{\text{synch}}(\nu) = \frac{1}{4\pi d^2} \int d^3r j_{\text{synch}}(\nu, r), \quad (4.12)$$

where d is the distance to the UFD and the integration is over the whole diffusion volume.

It is worth remembering that, unlike in the case for gamma rays, the synchrotron flux is not related to the J -factor, especially on account of the dependence on the diffusion and energy loss processes. Rather, the magnetic field B inside the UFD as well as the diffusion coefficient (parameterized by D_0 and γ_D) are the important attributes.

The magnetic field in the interior of a dSph is neither well understood nor well-measured. Rather, ranges for it are inferred using a variety of theoretical arguments [116]. Typically, star-forming low-mass galaxies such as dwarf irregulars carry a magnetic field of $\mathcal{O}(1-10)\mu\text{G}$, and this gives an order of magnitude estimate. This could be further refined by examining the observed correlations between the magnetic field and the star formation rate in Local group galaxies [117]. An independent source of the magnetic fields could be the Milky Way itself; large outflows of the galactic field have been observed [118], and these could well magnetize the dSphs. To circumvent the uncertainties associated with such modelling exercises, it has been suggested to use local equipartition between the magnetic field and the charged particles in the plasma (as evinced from cosmic rays). Each such mechanism indicate different preferred ranges, typically within an order of magnitude of $1\mu\text{G}$, often at slight variance with each other [116]. A further complication is introduced by the fact that the magnetic field can have a nontrivial profile. If the magnetic field owes its origin to the stars of the dSph, then it stands to reason that the field configuration would be maximum close to the center and decaying outwards. Certain studies have assumed an exponential profile having spherical

symmetry and of the form $B = B_0 e^{-r/r_*}$, where r_* would be of the order of the half-light radius of the dSph [69, 93, 116, 119, 120]. On the other hand, if the dSph is primarily magnetized by the Milky Way magnetic field, then the magnetic field would be expected to be almost constant over the dSPh, owing to the smallness of the latter’s size in comparison to its distance from Milky Way. Given these uncertainties, we assume a uniform profile of strength $B = 1 \mu\text{G}$ [32, 115] for most of our indicative calculations and discuss the variation of our result on the size and profile of the magnetic field strength in Sec. 5.

The diffusion coefficient, for which we assume the simplified form of eqn.4.4, has large uncertainties. For galaxy clusters, a value for the coefficient D_0 as large as 10^{28} – $10^{30} \text{ cm}^2/\text{s}$ has been argued for [91, 121]. Constraints on the Milky Way diffusion parameters can be inferred from data [122–124] and typically range between 10^{27} – $10^{29} \text{ cm}^2/\text{s}$. Similarly, the parameter γ_D is expected to lie in the range $0 \leq \gamma_D \leq 1$ [91]. To be specific, we choose values close to the geometric means of the individual ranges, namely $D_0 = 3 \times 10^{28} \text{ cm}^2/\text{s}$ and $\gamma_D = 0.3$ [93], postponing the discussion of the dependence on the choices to Sec.5.

For a given DM particle, the synchrotron flux, understandably, depends on the states to which it pair-annihilates and their subsequent cascades. As in the preceding sections, we consider three annihilation channel states, *i.e.*, $b\bar{b}$, $\tau^+\tau^-$ and $\mu^+\mu^-$, and for the sake of simplicity, continue to assume that a single channel dominates overwhelmingly. While we use the RX-DMFIT code [93] to calculate the synchrotron flux, it is useful to undertake a simplified discussion to understand the different aspects of the dynamics. For this exercise, we use a typical value for the velocity averaged DM annihilation cross section, namely, $\langle\sigma v\rangle = 10^{-26} \text{ cm}^3/\text{s}$, postponing a derivation of constraints on the same until later. For all the UFDs we have used a thermal electron density $n \approx 10^{-6} \text{ cm}^{-3}$ [32, 93], and the NFW density profile for the DM distribution within.

Fig.5 shows the stationary electron distribution spectrum for Tucana II at a radial distance 0.1 kpc for two different DM mass values, 200 GeV and 2 TeV. With the cascades from a b -decay being capable of producing more e^\pm than a τ or a μ can (the latter, only one), it is understandable that the integrated spectrum is much larger for the $b\bar{b}$ channel than it is for the others. The existence of the cascades also explains the relative softness of the three spectra in Fig.5.

For a given frequency, the energy corresponding to the peak of the synchrotron power spectrum contributes significantly to $j_{\text{synch}}(\nu, r)$ in eqn.4.11. The power spectrum $P_{\text{synch}}(\nu, E, B)$ for $B = 1 \mu\text{G}$ and for different frequencies in the range 5 MHz–50 GHz are shown in Fig.6a. Understandably, for higher frequencies, the synchrotron power peaks at a higher value of energy. Clearly, for a given frequency, the channel resulting in a larger number of e^\pm with energies closer to the peak of the synchrotron power spectrum will result in a larger syn-

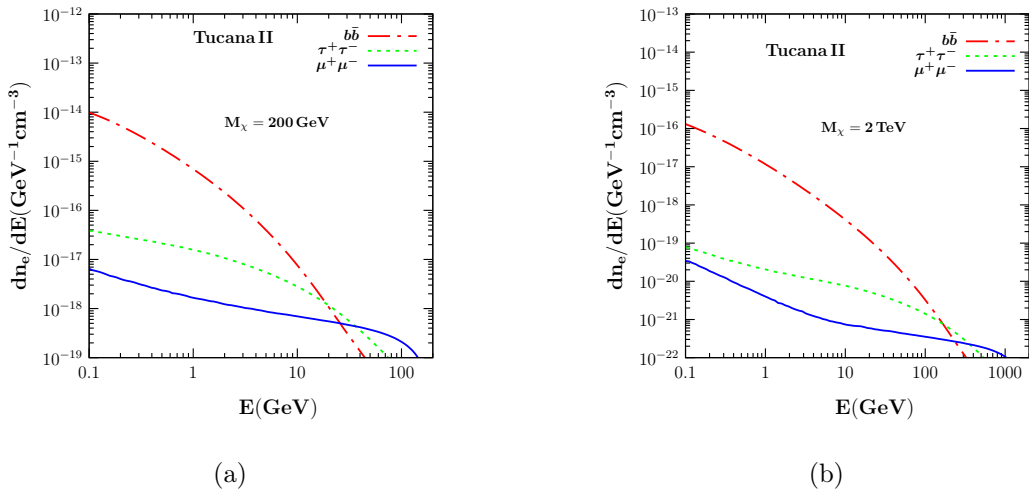


Figure 5: Equilibrium electron number density spectrum at a radial distance $r = 0.1$ kpc for Tucana II for three different exclusive annihilation channels, to $b\bar{b}$ (red), to $\tau^+\tau^-$ (green) and to $\mu^+\mu^-$ (blue), using $B = 1 \mu\text{G}$, $D_0 = 3 \times 10^{28} \text{ cm}^2/\text{s}$, $\gamma_D = 0.3$ and $\langle\sigma v\rangle = 10^{-26} \text{ cm}^3/\text{s}$ and the NFW density profile. The two panels correspond to different values for the DM mass.

chrotron flux. Hence, for higher frequencies, the synchrotron flux from a leptonic channel will dominate over that from a hadronic channel. This feature can be observed in Fig.6b where, for a given DM mass (*e.g.*, 200 GeV), the $\tau^+\tau^-$ channel dominates over the $b\bar{b}$ channel for higher frequencies; by the same token, for lower frequencies, the $b\bar{b}$ channel dominates over the $\tau^+\tau^-$ channel. Since the electrons originating from the pair-annihilation of a DM of mass M_χ can have a maximum energy M_χ , the spectrum corresponding to a heavier DM would be harder (as shown by Fig.5). Consequently, for larger frequencies, the synchrotron power spectrum peaks at a higher value of the electron energy. This is reflected in Fig.6b where, for a larger M_χ , the crossover from $b\bar{b}$ dominance to $\tau^+\tau^-$ dominance occurs at progressively higher frequencies.

4.1 Results pertaining to the Ultra Faint Dwarf Galaxies

We begin by considering existing radio-frequency observatories, in particular the data from the following two telescopes:

- the Giant Metrewave Radio Telescope (GMRT) [125] with its sky-survey, covering the expanse over -53° to $+90^\circ$, with a particularly useful set corresponding to $\nu = 0.1475$ GHz, and
- the NVSS survey by the Very Large Array (VLA) telescope [126], ranging over -40° to $+90^\circ$, and at $\nu = 1.4$ GHz.

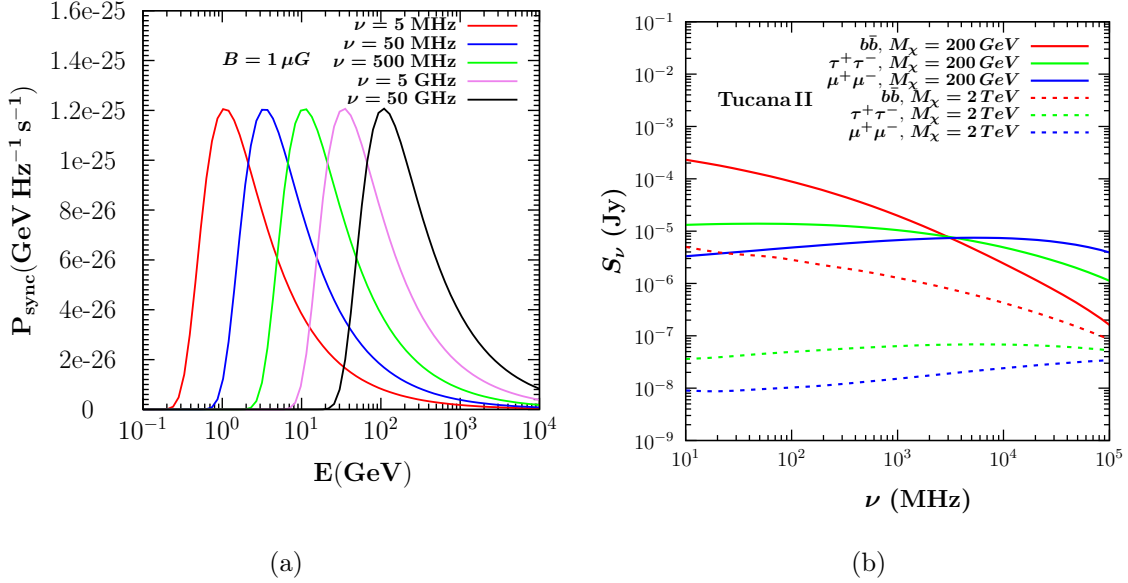


Figure 6: (a) Synchrotron power spectra at different frequencies for an arbitrary galaxy with a magnetic field $1 \mu\text{G}$. (b) Synchrotron fluxes for three exclusive final states for DM annihilation, i.e., $b\bar{b}$ (red), $\tau^+\tau^-$ (green) and $\mu^+\mu^-$ (blue). The solid (dashed) lines correspond to DM masses of 200 GeV and 2 TeV respectively. We have used $B = 1 \mu\text{G}$, $D_0 = 3 \times 10^{28} \text{ cm}^2/\text{s}$, $\gamma_D = 0.3$, $\langle\sigma v\rangle = 10^{-26} \text{ cm}^3/\text{s}$ and the NFW density profile for DM distribution inside the UFD.

The non-detection of radio emission from any of the UFDs can be translated to 95% C.L. upper limits on the fluxes ⁷ as listed in Table 3. Note here that the limited sky coverage implies that no statement can be made for certain UFDs, such as Tucana II.

These limits can, then, be translated to upper limits on $\langle\sigma v\rangle$ for different annihilation channels, as shown in Figure 7. As with the case of the gamma-ray observations, no such limit can be derived for Hydra II and Triangulum II as current observations only admit upper limits on their NFW density parameter ρ_s (see Table 1).

The comparison between the GMRT and the VLA results should be made carefully. For a given UFD, the limits obtained from VLA are, typically, stronger compared to those obtained from the GMRT. This is particularly true for larger M_χ . This is primarily because at lower frequencies in which GMRT operates, the rms noise is higher owing to radio interference and atmospheric turbulence. Additionally, at higher operating frequency the galactic backgrounds are smaller. On the other hand, at low M_χ , the situation reverses somewhat. This, again,

⁷Since all radio interferometric maps are made per unit beam where the beam is convolved with the respective point spread functions (PSF), we can directly obtain the flux density by using the final image.

Galaxy	GMRT ($\nu = 147.5$ MHz)	VLA ($\nu = 1.4$ GHz)
Aquarius II	6.8	0.86
Draco II	9	1.1
Eridanus II	7.8	No Data
Grus I	4.1	No Data
Hydra II	8.8	1.1
Leo V	6	0.98
Pegasus III	10	0.96
Pisces II	3.5	0.88
Triangulum II	6	1
Draco	7.2	9.2

Table 3: 95 % C.L. upper limits (in units of mJy) on the radio flux density from the UFDs obtained from GMRT and VLA. For Carina II, Horologium I, Reticulum II and Tucana II&III, neither observatory provides any data.

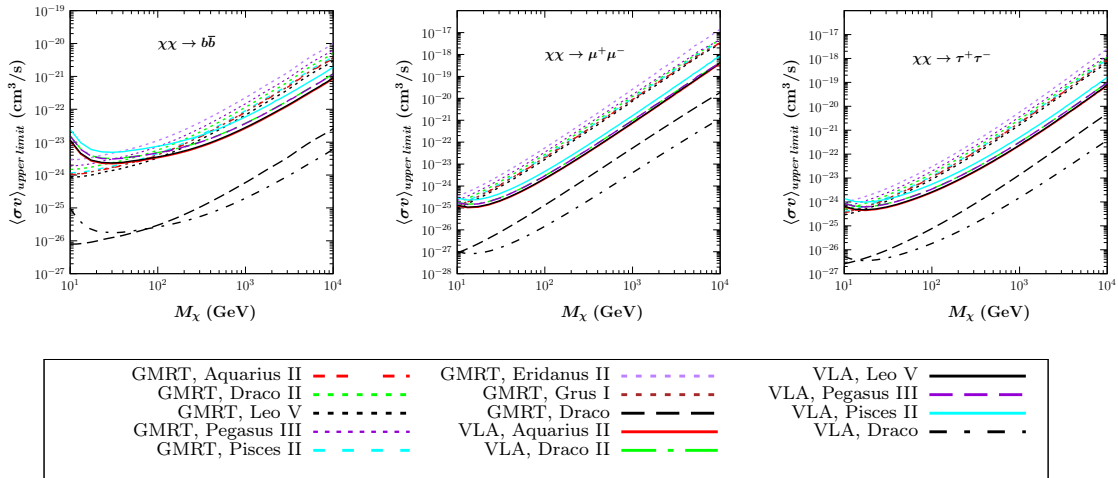


Figure 7: 95 % C.L. upper limits on $\langle\sigma v\rangle$ for different values of DM mass obtained using data from GMRT and VLA. The left, center and right panels are for $\chi\chi \rightarrow b\bar{b}$, $\tau^+\tau^-$, $\mu^+\mu^-$ respectively. We have used $B = 1 \mu G$, $D_0 = 3 \times 10^{28} \text{ cm}^2/\text{s}$, $\gamma_D = 0.3$ and the NFW density profile for the DM distribution inside the UFDs, with the values of the parameters d , r_h , ρ_s and r_s taken from Table 1.

is a consequence of the dependence of the synchrotron spectrum on M_χ and the relative efficiencies of the two telescopes.

4.2 Future projections

The Square Kilometer Array (SKA) is the largest radio telescope ever planned and the search for particulate DM is one of the primary goals of the project [20, 127]. We exploit the wide radio frequency range (50 MHz—50 GHz) of the SKA to examine its sensitivity to synchrotron emissions resulting from DM annihilations in the UFDs. To facilitate a qualitative comparison, we present, in Fig.8, the resultant synchrotron fluxes for each of three exclusive annihilation channels ($b\bar{b}$, $\tau^+\tau^-$ and $\mu^+\mu^-$). To this end, we have used a reference value of $\langle\sigma v\rangle = 10^{-26} \text{ cm}^3/\text{s}$, consistent with the upper limits obtained earlier. Once again, of the UFDs listed in Table 1, we do not consider Hydra II, Tucana III and Triangulum II as only upper limits on ρ_s are available for these. It should be noted that the wide angular coverage of the SKA implies that, unlike in the cases the GMRT or the VLA, none of the other UFDs need to be discounted. Also shown in Fig.8 are the predicted SKA sensitivities [128, 129] corresponding to three different exposure times, *viz.* 10, 100 and 1000 hours.

As we go to higher DM mass, two effects become more important. For one, the relic number density would fall, leading to a smaller rate of annihilation (since it scales as the square of the number density) for the same annihilation cross section. In addition, very energetic primaries leads to a harder synchrotron spectrum, thereby going beyond the sensitivity range of the SKA (just as very low frequencies are not well-suited for the SKA). Consequently, the feasibility of detecting radio signals at the SKA would decrease. As Fig.8 demonstrates, the synchrotron radiation from a 200 GeV DM pair-annihilating to any one of the three channels $b\bar{b}$, $\mu^+\mu^-$ and $\tau^+\tau^-$ from each of the 12 UFDs would be detectable with just 100 hours of SKA data (for an individual UFD, however, it could be much less). For $M_\chi = 2 \text{ TeV}$, though, even with 1000 hours of data, detection is guaranteed only for the $b\bar{b}$ channel. Interestingly, it is only for the classical dwarf galaxy Draco, that detection is assured for each of the three channels, and that too with only ~ 10 hours of SKA data. This is in stark contrast to the case of γ -ray signal at Fermi-LAT where several of the UFDs proffer better prospects than Draco.

5 Astrophysical Uncertainties and the Constraints

The constraints derived thus far have all been based on ‘central’ values of the various astrophysical parameters. In view of the rather restrictive nature of these constraints and even more so, the apparent sensitivity of future observatories such as the SKA, it behoves us to examine how crucially the said constraints depend on the exact values of the parameters.

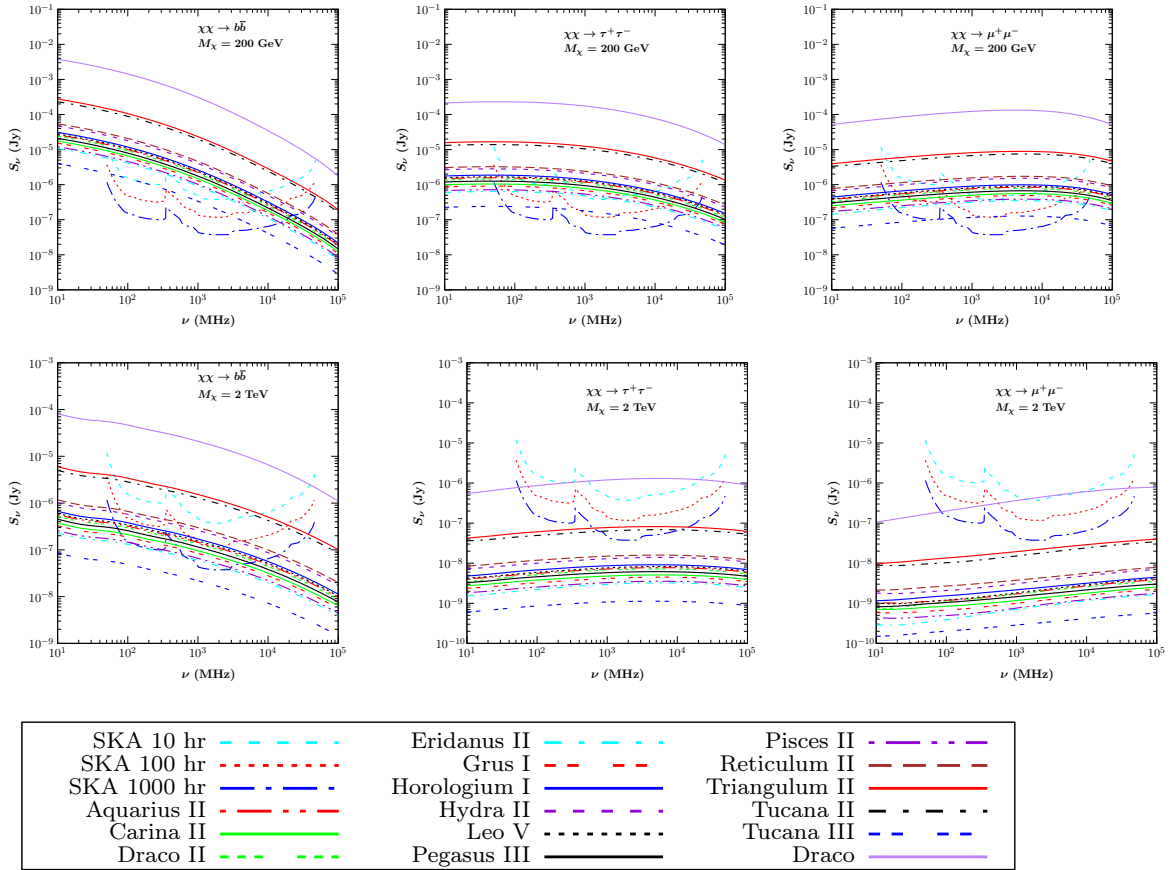


Figure 8: Synchrotron fluxes from the new galaxies including Draco. The left, center and right panels are for $\chi\chi \rightarrow b\bar{b}$, $\tau^+\tau^-$, $\mu^+\mu^-$ respectively, while the top (bottom) rows correspond to $M_\chi = 200\text{GeV}(2\text{TeV})$. For each plot $B = 1\mu\text{G}$, $D_0 = 3 \times 10^{28}\text{ cm}^2/\text{s}$, $\gamma_D = 0.3$ and $\langle\sigma v\rangle = 10^{-26}\text{ cm}^3/\text{s}$ have been used. NFW density profile has been used for DM distribution inside the UFDs. For each UFD the values of the parameters d , r_h , ρ_s and r_s have been used from Table 1. Since upper limits on ρ_s are available for Hydra II, Tucana III and Triangulum II (see Table 1), the corresponding curves for these three UFDs show the maximum possible amount of synchrotron flux.

This assumes particular significance in view of the fact that, for several of the astrophysical measurements, the uncertainties are significantly large.

5.1 Uncertainties in the Gamma-Ray bounds

A prime source of errors is, of course, the DM distribution. With very few visible stars in the UFDs, the kinematic data is sparse[85] and this has proved an obstacle in understanding the DM distribution in UFDs. Indeed, while N -body simulations seem to argue for the NFW

distribution, the data has also been interpreted to favour isothermal distributions [100]. Since Horologium I had led to the strongest constraints, we choose to illustrate the role of the density profile for this particular UFD. Using the central values for the J -factor from Table 2, we depict, in Fig. 9, the consequent upper limits on $\langle\sigma v\rangle$ for all three density profiles. For brevity's sake we only present the results for $b\bar{b}$ channel alone, with the understanding that the relative change in the constraints are entirely analogous for the two other channels. It is worthwhile to note that the Burkert profile would have led to stronger constraints than we have, while the isothermal-like profiles would, typically, lead to weaker constraints. This feature repeats for most other UFDs as well.

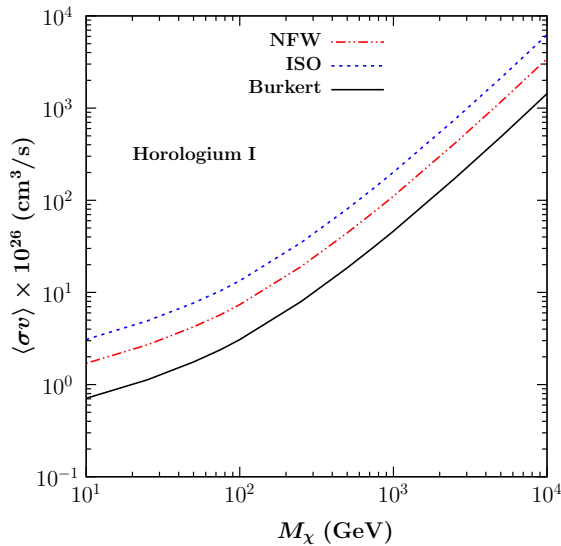


Figure 9: Comparison between the $\langle\sigma v\rangle$ upper limits for three density profiles for 100% $b\bar{b}$ final state.

This dependence can be recast in terms of the uncertainties in the J -factor. Indeed, in the context of the γ -ray signal, ambiguities in the density profile can be subsumed, to a great extent, in uncertainties in the J -factor. Indeed, while the J -factor corresponding to the NFW profile gives the median value, a look at Table 2 convinces us that the central values associated with the two other profiles do fall within the 1σ band of the former. With the γ -ray flux being proportional to the J -factor (see eqn.2.1), it is understandable that a large error in the latter would translate to correspondingly large errors in the upper limit on $\langle\sigma v\rangle$. As the dependences are straightforward, we do not discuss these any further.

5.2 Uncertainties in the synchrotron fluxes

As with the case for the gamma-ray fluxes, the synchrotron fluxes too are subject to uncertainties on account of the errors in determining the astrophysical parameters d (distance to the UFD), $r_{1/2}$ (its half-light radius) and the velocity-dispersion $\sigma_{l.o.s.}$. Using the 1σ uncertainties in these, as listed in Table A–I, we show, in Fig. 10, the consequent uncertainties in the synchrotron flux for a 200 GeV DM annihilating to $b\bar{b}$ final state in Tucana II. The choice of the particular UFD to demonstrate these effects is motivated by it being the one associated with the highest synchrotron flux. While the actual error would be a combination of all three contributions, in the absence of adequate information regarding the correlations between the same, we have not chosen to attempt this convolution. It should, nonetheless, be obvious that with the relative error in d already being small, a further improvement in this measurement is not crucial. With the relative error in the $r_{1/2}$ measurement being larger, this variable, quite expectedly, contributes more to the error. Understandably, much more crucial is the determination of the velocity dispersion, both on account of the current level of accuracy in its measurement and the particularly important role that this variable plays in determining the synchrotron spectrum.

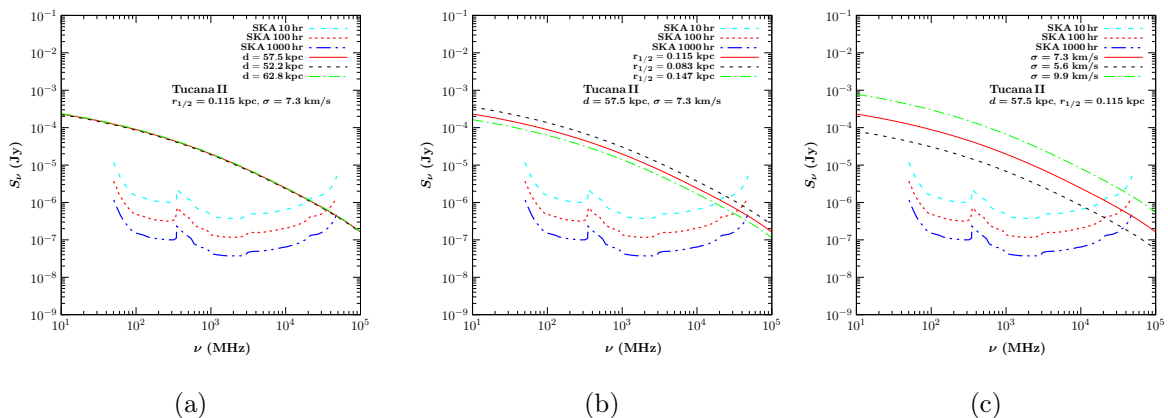


Figure 10: Individual contributions to the uncertainty in the synchrotron flux—resulting from a pair of 200 GeV DM particles in Tucana II annihilating into $b\bar{b}$ —due to 1σ uncertainties in the parameters (a) d , (b) $r_{1/2}$ and (c) $\sigma_{l.o.s.}$. We use the NFW profile along with $B = 1 \mu G$, $D_0 = 3 \times 10^{28} \text{ cm}^2/\text{s}$, $\gamma_D = 0.3$ and $\langle\sigma v\rangle = 10^{-26} \text{ cm}^3/\text{s}$.

As with the gamma-ray fluxes, the lack of precise knowledge of the DM density distribution leads to substantial uncertainties. While we have, until now, used the NFW profile, in Fig. 11 we display the differences in predicted flux for Tucana II for NFW, Burkert and ISO profiles. It is interesting to note that while, for the gamma-ray flux, the NFW profile closely corresponded to the median prediction, in the present context it leads to the highest

fluxes, while the Burkert profile leads to the lowest. Fortunately enough, the difference between the predictions for theoretically favoured NFW profile and the observationally favoured isothermal profiles is not very significant, thereby maintaining the robustness of our results.

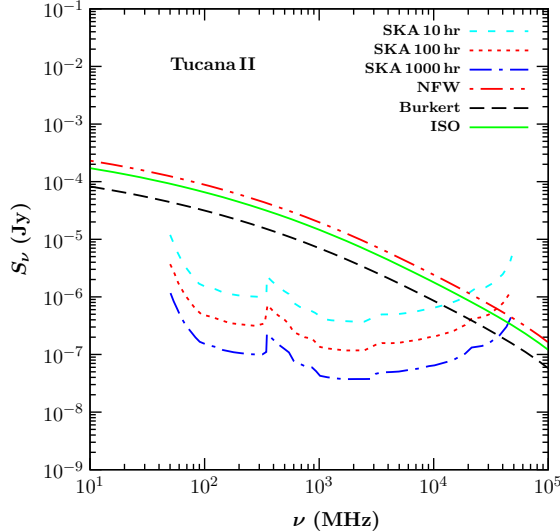


Figure 11: *Synchrotron flux vs. frequency for Tucana II for different dark matter distribution profiles : NFW, Burkert and ISO. We have considered a 200 GeV DM annihilating to $b\bar{b}$ final state, as also $B = 1 \mu\text{G}$, $D_0 = 3 \times 10^{28} \text{ cm}^2/\text{s}$, $\gamma_D = 0.3$ and $\langle\sigma v\rangle = 10^{-26} \text{ cm}^3/\text{s}$.*

Much more crucial is the dependence on the diffusion parameter $D(E)$, which too is not known precisely. In Section 4, we had indicated the typical ranges of the diffusion constant D_0 and exponent γ_D , but effected our numerical analysis with ‘central’ values alone. In view of the fact even the probability distributions for these parameters are not well known, “ 1σ ” intervals are not well-defined. Hence, in Fig.12, we plot the synchrotron fluxes for the entire plausible ranges of these parameters, $D_0 \in [3 \times 10^{26}, 10^{30}] \text{ cm}^2/\text{s}$, and $\gamma_D \in [0.1, 1]$. A smaller value for D_0 would allow the e^\pm to see the magnetic field of the UFD for a longer duration resulting in a larger synchrotron flux. The overall dependence is close to being a linear one (see Fig. 12a). As for γ_D , the very definition (eqn. 4.4) stipulates that a larger value enhances (suppresses) $D(E)$ for $E(e^\pm) > 1 (< 1)$. Since high-frequency synchrotron photons would preferentially be radiated by high-energy e^\pm (see Fig. 6a), a larger γ_D would progressively suppress the synchrotron flux at higher frequencies; similarly, substantially below $\nu \sim 1 \text{ MHz}$, the flux would be enhanced. The region $\nu \in (1, 5) \text{ MHz}$ roughly corresponds to the peak for $E(e^\pm) = 1 \text{ GeV}$ (see Fig. 6a) and, understandably, the effect is relatively small in this region (see Fig. 12b).

Finally, we come to the elephant in the room, namely the size and the profile of the

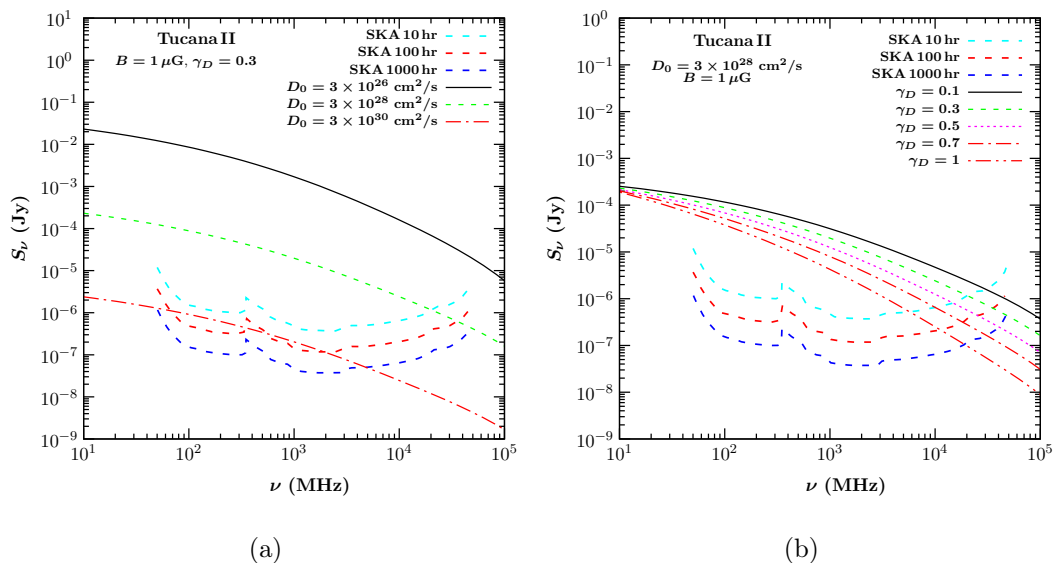


Figure 12: Synchrotron flux versus frequency for different values of (a) D_0 and (b) γ_D . The mass of DM is 200 GeV and the DM pair annihilates to $b\bar{b}$ final state with $\langle\sigma v\rangle = 10^{-26} \text{ cm}^3/\text{s}$. NFW density profile has been used for DM distribution inside the UFD.

magnetic field. In Section 4, we had discussed the uncertainties in these and indicated the typical ranges of the field B . Once again, eschewing “ 1σ ” intervals, and concentrating first on a flat magnetic field, we plot, in Fig.13a, the synchrotron fluxes for the entire plausible range *viz.*, $B \in [0.5, 10] \mu\text{G}$. With the magnetic field driving the synchrotron radiation, the strong dependence of the flux (see Fig. 13a) is understandable. Indeed, for small frequencies, the flux is nearly proportional to B , with the dependence growing significantly stronger at larger frequencies, an effect that is easily understood in term of classical electrodynamics.

While a majority of DM studies have considered a flat magnetic field profile within a dSph, the truth could be very different indeed. As discussed in Section 4, a popular choice (in the absence of more precise data or simulations) is to consider an exponential profile, *viz.* $B = B_0 e^{-r/r_*}$ with r_* being of the order of the half-light radius of the dSph [69, 93, 116]. Assuming such a profile, we study next the consequences for the same. To compare the results to those for a flat profile $B = B_{\text{av}}$, one needs to normalize appropriately and we do this by equating the average values, with the average taken over the entire diffusion zone, *viz.* $0 \leq r \leq r_h$. It should be obvious that, in view of the damping of the field, $\mathcal{O}(1)$ changes in the upper limit is of little consequence. Much more important is the value of r_* (and, here, we choose two representative values, namely $r_* = r_{1/2}$ and $r_* = 2r_{1/2}$) and the definition of the averaging. While equating the magnetic energies would require that $\langle B^2 \rangle \equiv V^{-1} \int d^3r B^2(r) = B_{\text{av}}^2$ (with V being the volume of the dSph), some analyses have

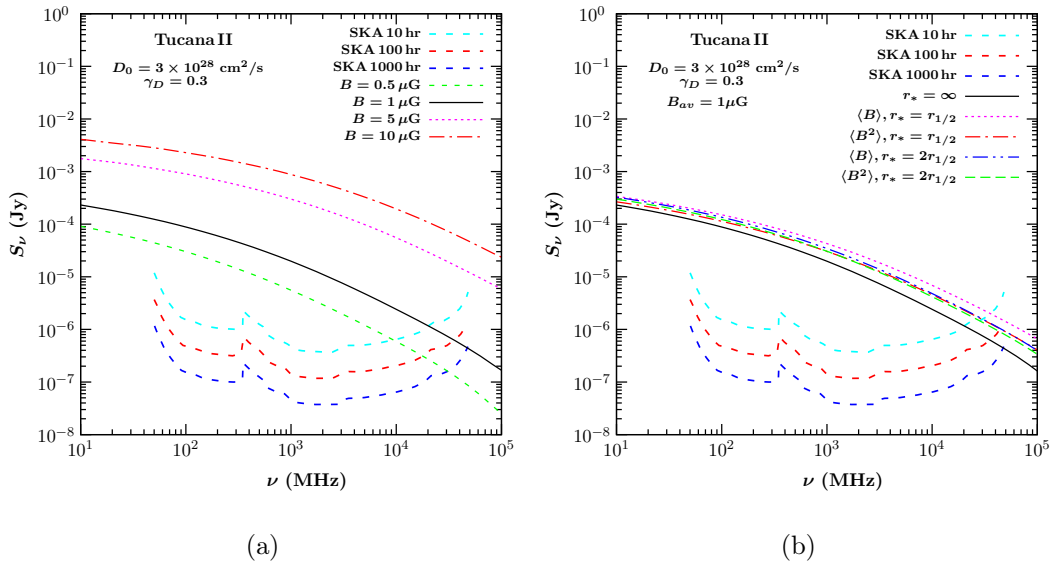


Figure 13: Synchrotron flux as a function of frequency, for $m_\chi = 200\text{GeV}$ with the DM pair annihilating to $b\bar{b}$ final state with $\langle\sigma v\rangle = 10^{-26}\text{ cm}^3/\text{s}$. The NFW density profile has been used for DM distribution inside the UFD. (a) For flat magnetic fields of different strengths. (b) Assuming a exponential profile for B maintaining an average (see text) of $1\mu\text{G}$.

used $\langle|B|\rangle = B_{\text{av}}$ instead, and hence we display results for both the definitions. As Fig.13b shows, for each such profile, the resultant flux would be larger than that obtained for the flat profile (namely, $r_* = \infty$) with the same average value. The reason is easy to divine. In each case, the central region of the galaxy is associated with a field larger than the average value. With the central region also being characterised by a larger DM (the progenitors of the charged particles) number density, it is conceivable that such profiles would lead to larger synchrotron fluxes. Such arguments, applied naively, would indicate that a smaller value for r_* should lead to a larger flux. However, it needs to be borne in mind that a very fast-falling magnetic field would also imply that only a small volume contributes to the flux. With a nontrivial energy dependence of dn_e^\pm/dE and an even more complicated form of the synchrotron power spectrum (see Sec.4), the resultant convolution should not be expected to follow the aforementioned naive argument. Nonetheless, it is well-satisfied in the case of averaging $\langle|B|\rangle$. If the averaging algorithm involves $\langle B^2\rangle$, the dependence of S_ν on the value of r_* is relatively muted, and there is a crossover at $\nu \sim 1\text{ GHz}$.

6 Discussions and Conclusions

Dwarf spheroidal galaxies, apart from being dominated by dark matter, have almost no millisecond pulsars, and yet possess considerable large scale magnetic fields. These render them

ideal arenas for indirect detection of dark matter through photonic signals. Several attempts have been made recently to derive strong bounds on annihilation cross sections of dark matter using both gamma rays and radio observations [19, 71–79, 119, 120, 130, 131]. Most of the early observations concentrated on the dwarf spheroidal galaxies of the Local group. Our work has been primarily motivated by the new class of UFDs discovered in the past years using data from Pan-STARRS, Dark Energy Survey and a few other surveys. In this paper, we have studied such signals in two distinct parts of the electromagnetic spectrum, namely high energy gamma rays on the one hand and radio signals on the other. We have performed a search for signatures of particle DM annihilations in 15 UFDs using data from the Fermi-LAT. Additionally we have also searched for synchrotron radiation from high-energy electrons and positrons originating from DM annihilations from these objects using GMRT and VLA. We have also estimated the spectra of the radio signals and compared their detectability with the upcoming Square Kilometer Array (SKA) in the frequency range 50 MHz to 50 GHz.

Eleven years of gamma-ray data collected by the Fermi-LAT collaboration has failed to show any significant excess from any of the fifteen ultra faint dwarf spheroidal galaxies. The stringent upper limits on the γ -ray flux that these null-results imply are translated to upper limits on the thermal average of the pair annihilation cross section $\langle\sigma v\rangle$, for a given value of DM mass. We have done this for 12 of the UFDs. As for the remaining three (viz. Triangulum-II, Hydra-II and Tucana-III), since only upper limits on the corresponding (astrophysical) J -factors are available, it is not possible to use these three to obtain robust upper limits on $\langle\sigma v\rangle$.

The DM could, of course, annihilate into a plethora of channels, with the relative probabilities having a strong dependence on the underlying dynamics governing the system. Rather than be slave to a particular model, we consider instead that the pair annihilation proceeds *exclusively* through one of three channels, viz., $b\bar{b}$, $\tau^+\tau^-$ and $\mu^+\mu^-$. The ensuing independent constraints can, then, be combined to constrain the parameter space of any model where the annihilation is dominated by one of the three channels. Indeed, simple scaling arguments can also be used to infer bounds applicable for annihilations into other light fermions.

As far as the gamma-ray signal is concerned, of all the dwarf galaxies, Holmberg-1 imposed the most stringent limits, and, for the $b\bar{b}$ channel, easily outdoes the limits obtained by the Planck collaboration [114]. It needs to be said here that the limits obtained by us have a significant dependence on the DM density profile. While most of our results were derived using the NFW profile, we have considered the Burkert and ISO profiles as well. In general the Burkert profile led to the strongest bounds on $\langle\sigma v\rangle$ and the ISO the weakest. Our limits, thus, represent, typically, the middle-of-the-road constraints. We also performed a stacking analysis where we have generated a joint likelihood function as a product of individual

likelihood functions of UFDs. We found that the stacking analysis improves the combined limits modestly as compared to the limits obtained from the few best individual UFDs alone. For brevity's sake, we do not present here a figure for the same.

A further source of photons is the synchrotron radiation, largely from electrons/positrons resulting from the aforementioned DM annihilations (produced either directly or as the end product of cascades for annihilations into heavier Standard Model particles). Emitted as the e^\pm travel through the magnetic field of the UFDs, the synchrotron radiation, typically, falls in the radio frequency range. We have calculated the upper limit on DM annihilation cross section for different annihilation final states, i.e., $b\bar{b}$, $\tau^+\tau^-$ and $\mu^+\mu^-$ for the UFDs using the available radio flux upper limits from the GMRT and VLA telescope data. The rms sensitivity of the observations range from about a few mJy for GMRT at 147 MHz to few hundreds of μ Jy for VLA at 1.4 GHz for all the targets of observations. Comparing these results with those obtained from the Fermi-LAT data, we have found that it is the VLA that imposes the strongest constraints. This holds for a wide range of DM masses, not merely the representative values of 200 GeV and 2 TeV that we have used to depict our results.

Turning to the near future, we consider the synchrotron fluxes, over a wide frequency range (10 MHz to 100 GHz) for a low annihilation cross section ($\langle\sigma v\rangle = 10^{-26}$ cm³/s) and a low magnetic field ($B = 1\mu$ G) and a typical diffusion coefficient ($D_0 = 3 \times 10^{28}$ cm²/s) and index ($\gamma_D = 0.3$). Comparing these with the (frequency-dependent) sensitivity of the SKA telescope, we have found that for a DM of mass 200 GeV pair-annihilating into $b\bar{b}$, even a 10 hour exposure would be enough to detect a signal from each of the UFDs. For annihilations into $\tau^+\tau^-$ or $\mu^+\mu^-$ pairs, the fluxes are lower, but 100 hours worth of data should suffice. On the other hand, for much heavier DM (say, a mass of 2 TeV), the number density is smaller, and, furthermore, the spectrum of the synchrotron radiation is harder. Consequently, a significantly longer exposure would be needed. For example, for annihilations into a $b\bar{b}$ pair, a 10 hour exposure would now suffice only for Triangulum II and Tucana II (apart from the classic Draco, of course), with 100 hours being sufficient for the rest. On the other hand, for such heavy DM annihilating into $\tau^+\tau^-$ or $\mu^+\mu^-$, even an exposure of 1000 hours would be barely enough.

Such quantitative conclusions depend, of course, on the annihilation rate $\langle\sigma v\rangle$ and it should be appreciated that we have assumed values significantly lower than that allowed currently. Also to be remembered is that the fluxes have significant dependences on many astrophysical parameters that are, yet, not very well-measured. Investigating the effects of these, we conclude that the strength of the magnetic field (inside the UFD) and the diffusion coefficient D_0 are the parameters that need to be better measured with the velocity dispersion of the DM being the other critical observable. Unlike high energy gamma-rays,

these synchrotron radiations are strongly dependent on the magnetic field and the diffusion coefficient via the diffusion process of the electrons through the inter-galactic medium. The current knowledge of magnetic field and the diffusion coefficient for the UFDs are not very precise. We have studied the dependence of synchrotron flux on B , D_0 and γ_D for a 200 GeV DM annihilating to $b\bar{b}$ final state in Tucana II. We have found that the flux changes significantly with the variation of these parameters. Moreover, the amount of synchrotron flux depends on the choice of DM profile for a given UFD. For Tucana II we compared the flux for NFW, Burkert and ISO profiles, and found that NFW profile provides largest amount of flux among the three. For the newly discovered UFDs, large uncertainties are present in the measured values of the astrophysical parameters such as the half-light radius ($r_{1/2}$), heliocentric distance (d) and velocity dispersion ($\sigma_{l.o.s}$). The radius of the diffusion zone (r_h) and the parameters of the DM profile also depend on these astrophysical parameters, hence affecting the synchrotron flux from a UFD. We have studied the uncertainty in synchrotron flux due to uncertainty in these parameters. We have found that uncertainty in flux is largest due to uncertainty in velocity dispersion compared to uncertainty in half-light radius and heliocentric distance.

Despite these uncertainties, it can, thus, be safely concluded that we are about to enter a very interesting era of indirect detection of DM. A particularly important conclusion is that, even a photonic signal is best searched for by a combination of multiple telescopes working at very disparate wavelengths. This is exemplified by Fig. 14 which shows the comparison between the best limits from VLA with the best from Fermi-LAT for all the three annihilation channels. It is interesting to note that while, for Fermi-LAT, it is Horologium I that provides the best limit, for the VLA, it is Draco that does so. Furthermore, over the wide mass range $M_\chi \in (10, 10^4)$ GeV, if the DM annihilates preferentially to $\mu^+\mu^-$ or $\tau^+\tau^-$, then it is the VLA that has a better sensitivity, while if the preferred channel is $b\bar{b}$ instead, Fermi-LAT is likely to prove a better bet.

It is heartening to note that apart from collecting a much increased amount of data, the Fermi-LAT collaboration is already engaged in efforts that would allow it to perform improved event selection with larger collection area [102]. Furthermore, multi-target multi-instrument searches for gamma-ray signals from annihilation of dark matter particles in the mass between 10 GeV and 100 TeV [22] are in the offing. Such an approach can provide rather stringent limits on the cross sections for dark matter particles and has the ability to probe the widest range of masses. In the near future, the next generation ground based atmospheric Cerenkov telescope array (CTA) will be operational and is expected to have an unprecedented sensitivity over a very wide range of energy from few tens of GeV to hundreds of TeV [132] and will have the potential to probe the thermal relic interaction rate in various

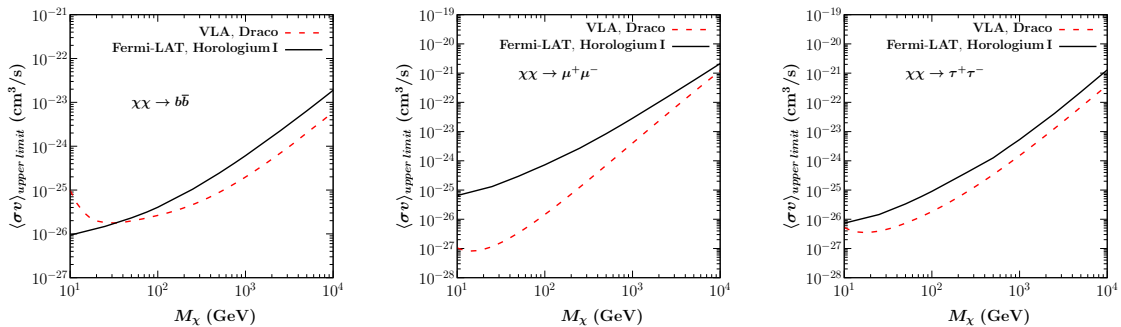


Figure 14: Comparison of 95 % C.L. upper limits on $\langle\sigma v\rangle$ from VLA and Fermi-LAT. We have compared the best limit from VLA (Draco) with the best limit from Fermi-LAT (Horologium I). The left, center and right panels are for $\chi\chi \rightarrow b\bar{b}$, $\tau^+\tau^-$ and $\mu^+\mu^-$ respectively. The VLA limit for Draco has been obtained with the astrophysical parameters $B = 1 \mu G$, $D_0 = 3 \times 10^{28} \text{ cm}^2/\text{s}$ and $\gamma_D = 0.3$. NFW density profile has been used for DM distribution inside the UFD.

astrophysical objects. At the same time, radio astronomy is entering into a golden era with the Square Kilometer Array (SKA) project expected to complete the Phase-I construction of the world’s largest radio telescope array soon and further improve the sensitivity and spectral range in Phase-2 in future. Along with its pathfinders ASKAP and MeerKAT as also Low-Frequency Array (LOFAR) which have started operation, multifarious search strategies can be undertaken. All these telescope arrays will be able to reach a sensitivity of a few μJy rms noise level in only a few hours of observation time. Finally, SKA will have ~ 10 times increase in sensitivity from few tens of MHz to 50 GHz and such a wide frequency coverage will be important for putting constraints on dark matter particle mass. Furthermore SKA will also have the capability to measure the magnetic field in many dSphs via Faraday rotation measurements which will help one to make more robust predictions for the expected dark matter induced synchrotron radiation.

It is also worthwhile to consider that, were DM signals to be confirmed by other independent experiments, the signal (or lack thereof) in future radio-frequency (or gamma-ray) observatories could, in principle, be used to probe properties (such as magnetic fields, diffusion parameters and the DM density distribution) of the dwarf spheroidals.

Note added: After this paper was completed, ref.[133] appeared, claiming to have corrected an error in the Green’s function (see eqn.4.6) used so far in the literature. We have recomputed S_ν with the Green’s function advocated in ref.[133], and find that while it is now enhanced slightly for small ν , it is suppressed by about 40% at the very largest of frequencies. Overall, there

would be only a small change in the outcome, distinctly smaller than the other uncertainties that we have listed.

Acknowledgments

The authors would like to thank Alex McDaniel for providing us the most recent version of the RX-DMFIT code & various clarifications regarding the use of this code, and Stefano Profumo for discussions on diffusion radii for UFDs. PB thanks Mousumi Das for helpful discussions on radio analysis. KD would like to thank Marco Cirelli and Arpan Kar for useful discussions. The work of PB is supported by the DST INSPIRE Fellowship Scheme, India. DC acknowledges research grant CRG/2018/004889 of the SERB, India.

A Source details

We revisit here the dwarf spheroidal galaxies considered in our study, chosen on account of their very high mass to light ratio and moderately large velocity dispersion of the stars therein, each of which points to the conclusion that these UFDs are likely to be very rich in dark matter content [134]. The corresponding spectroscopic and the photometric studies are mentioned in Table A–I, where the quantities M/L , d , $r_{1/2}$ and $\sigma_{l.o.s}$ denote the mass to light ratio, the heliocentric distance, the half-light radius and the velocity dispersion of each UFD galaxy. θ_{max}^o is the angle made by the outer most star of the UFD.

Galaxy	M/L (M_{\odot}/L_{\odot})	d (Kpc)	$r_{1/2}$ (pc)	$\sigma_{l.o.s}$ ($km\ s^{-1}$)	θ_{max}°
Aquarius II	1330^{+3242}_{-227}	$107.9^{+3.3}_{-3.3}$	123^{+22}_{-21}	$6.2^{+2.6}_{-1.7}$	0.11134
Carina II	369^{+309}_{-161}	$37.4^{+0.4}_{-0.4}$	77^{+8}_{-8}	$3.4^{+1.2}_{-0.8}$	0.23
Draco II	501^{+1083}_{-421}	$20.0^{+3.0}_{-3.0}$	12^{+5}_{-5}	$3.4^{+2.5}_{-1.9}$	0.1
Eridanus II	420^{+210}_{-140}	$366.0^{+17.0}_{-17.0}$	176^{+14}_{-14}	$7.1^{+1.2}_{-0.9}$	0.062
Grus I	< 2645	$120.2^{+11.1}_{-11.0}$	52^{+26}_{-26}	$4.5^{+5.0}_{-2.8}$	0.093
Horologium I	570^{+1154}_{-112}	$79.0^{+7.0}_{-7.0}$	32^{+5}_{-5}	$5.9^{+3.3}_{-1.8}$	0.0619
Hydra II	< 315	$151.0^{+8.0}_{-8.0}$	71^{+11}_{-11}	< 6.82	0.08509
Leo V	264^{+326}_{-264}	$173.0^{+5.0}_{-5.0}$	30^{+17}_{-17}	$4.9^{+3.0}_{-1.9}$	0.077
Pegasus III	1470^{+5660}_{-1240}	215.0^{+12}_{-12}	37^{+14}_{-14}	$7.9^{+4.4}_{-3.1}$	0.03049
Pisces II	370^{+310}_{-240}	183.0^{+15}_{-15}	48^{+10}_{-10}	$4.8^{+3.3}_{-2.0}$	0.06861
Reticulum II	467^{+286}_{-168}	30^{+2}_{-2}	32^{+3}_{-3}	$3.4^{+0.7}_{-0.6}$	0.24
Tucana II	1913^{+2234}_{-950}	$57.5^{+5.3}_{-5.3}$	115^{+32}_{-32}	$7.3^{+2.6}_{-1.7}$	0.225
Tucana III	< 240	25.0^{+2}_{-2}	43^{+6}_{-6}	< 2.18	0.2
Triangulum II	< 2510	30^{+2}_{-2}	28^{+8}_{-8}	< 6.36	0.15

Table A–I: *Properties of our selected UFD galaxies. Parameters d , $r_{1/2}$ and $\sigma_{l.o.s}$ has been collected from [92]. M/L and θ_{max}° has been collected from the references [135–147].*

B Parameters used in Science Tools

Parameter for data extraction ⁸	
Parameter	Value
Radius of interest (ROI)	15°
TSTART (MET)	241976960 (2008-09-01 15:49:19.000 UTC)
TSTOP (MET)	570987500 (2019-02-04 15:38:15.000 UTC)
Energy Range	100 MeV - 300 GeV
<i>Fermitools</i> version	1.2.1 ⁹
gtselect for event selection ¹⁰	
Event class	Source type (128) ¹¹
Event type	Front+Back (3) ¹¹
Maximum zenith angle cut	90° ¹¹
gtmktime for time selection ¹²	
Filter applied	(DATA_QUAL > 0)&&(LAT_CONFIG == 1) ¹³
ROI-based zenith angle cut	No ¹³
gtltcube for livetime cube ¹⁴	
Maximum zenith angle cut (z_{cut})	90° ¹⁵
Step size in $\cos(\theta)$	0.025
Pixel size (degrees)	1
gtbin for 3-D (binned) counts map ¹⁶	
Size of the X & Y axis (pixels)	140
Image scale (degrees/pixel)	0.1
Coordinate system	Celestial (CEL)
Projection method	AIT
Number of logarithmically uniform energy bins	24
gtexpcube2 for exposure map ¹⁷	
Instrument Response Function (IRF)	P8R3_SOURCE_V2 ¹⁸
Size of the X & Y axis (pixels)	400
Image scale (degrees/pixel)	0.1
Coordinate system	Celestial (CEL)
Projection method	AIT
Number of logarithmically uniform energy bins	24
diffuse models and Source model XML file ¹⁹	
Galactic diffuse emission model	gll_iem_v07.fits ²⁰
Extragalactic isotropic diffuse emission model	iso_P8R3_SOURCE_V2_v1.txt ²⁰
Source catalog	4FGL
Extra radius of interest	5°
Spectral model	DMFit Function[84] ²¹

Table A–II: *Parameters used in Science Tools for Fermi-LAT data analysis*

⁸https://fermi.gsfc.nasa.gov/ssc/data/analysis/scitools/extract_latdata.html
⁹<https://fermi.gsfc.nasa.gov/ssc/data/analysis/software/>
¹⁰<https://fermi.gsfc.nasa.gov/ssc/data/analysis/scitools/help/gtselect.txt>
¹¹https://fermi.gsfc.nasa.gov/ssc/data/analysis/documentation/Cicerone/Cicerone_Data_Exploration/Data_preparation.html
¹²<https://fermi.gsfc.nasa.gov/ssc/data/analysis/scitools/help/gtmktime.txt>
¹³https://fermi.gsfc.nasa.gov/ssc/data/analysis/scitools/data_preparation.html
¹⁴<https://fermi.gsfc.nasa.gov/ssc/data/analysis/scitools/help/gtlcube.txt>
¹⁵https://fermi.gsfc.nasa.gov/ssc/data/analysis/documentation/Cicerone/Cicerone_Likelihood/Exposure.html
¹⁶<https://fermi.gsfc.nasa.gov/ssc/data/analysis/scitools/help/gtbin.txt>
¹⁷<https://fermi.gsfc.nasa.gov/ssc/data/analysis/scitools/help/gtexpcube2.txt>
¹⁸https://fermi.gsfc.nasa.gov/ssc/data/analysis/documentation/Pass8_usage.html
¹⁹<https://fermi.gsfc.nasa.gov/ssc/data/analysis/user/make4FGLxml.py>
²⁰<https://fermi.gsfc.nasa.gov/ssc/data/access/lat/BackgroundModels.html>
²¹https://fermi.gsfc.nasa.gov/ssc/data/analysis/scitools/source_models.html

References

- [1] A.H. Peter, *Dark Matter: A Brief Review*, [1201.3942](#).
- [2] J.R. Primack, *Dark matter and structure formation*, in *Midrasha Mathematicae in Jerusalem: Winter School in Dynamical Systems*, 7, 1997 [[astro-ph/9707285](#)].
- [3] M. Lisanti, *Lectures on Dark Matter Physics*, in *Theoretical Advanced Study Institute in Elementary Particle Physics: New Frontiers in Fields and Strings*, pp. 399–446, 2017, DOI [[1603.03797](#)].
- [4] M.W. Goodman and E. Witten, *Detectability of certain dark-matter candidates*, *Phys. Rev. D* **31** (1985) 3059.
- [5] M. Schumann, *Direct Detection of WIMP Dark Matter: Concepts and Status*, *J. Phys. G* **46** (2019) 103003 [[1903.03026](#)].
- [6] XENON10 collaboration, *Limits on spin-dependent WIMP-nucleon cross-sections from the XENON10 experiment*, *Phys. Rev. Lett.* **101** (2008) 091301 [[0805.2939](#)].
- [7] XENON100 collaboration, *XENON100 Dark Matter Results from a Combination of 477 Live Days*, *Phys. Rev. D* **94** (2016) 122001 [[1609.06154](#)].
- [8] DAMIC collaboration, *Search for low-mass WIMPs in a 0.6 kg day exposure of the DAMIC experiment at SNOLAB*, *Phys. Rev. D* **94** (2016) 082006 [[1607.07410](#)].
- [9] PICO collaboration, *Dark Matter Search Results from the PICO-60 C₃F₈ Bubble Chamber*, *Phys. Rev. Lett.* **118** (2017) 251301 [[1702.07666](#)].
- [10] PANDAX-II collaboration, *Dark Matter Results From 54-Ton-Day Exposure of PandaX-II Experiment*, *Phys. Rev. Lett.* **119** (2017) 181302 [[1708.06917](#)].
- [11] LUX collaboration, *Limits on spin-dependent WIMP-nucleon cross section obtained from the complete LUX exposure*, *Phys. Rev. Lett.* **118** (2017) 251302 [[1705.03380](#)].
- [12] DARKSIDE collaboration, *Low-Mass Dark Matter Search with the DarkSide-50 Experiment*, *Phys. Rev. Lett.* **121** (2018) 081307 [[1802.06994](#)].
- [13] F. Kahlhoefer, *Review of LHC Dark Matter Searches*, *Int. J. Mod. Phys. A* **32** (2017) 1730006 [[1702.02430](#)].
- [14] N. Borodatchenkova, D. Choudhury and M. Drees, *Probing MeV dark matter at low-energy e^+e^- colliders*, *Phys. Rev. Lett.* **96** (2006) 141802 [[hep-ph/0510147](#)].
- [15] BELLE collaboration, *Search for a light CP-odd Higgs boson and low-mass dark matter at the Belle experiment*, [1809.05222](#).
- [16] D. Choudhury and D. Sachdeva, *Model independent analysis of MeV scale dark matter. II. Implications from e^-e^+ colliders and direct detection*, *Phys. Rev. D* **100** (2019) 075007 [[1906.06364](#)].

- [17] J. Buckley et al., *Working Group Report: WIMP Dark Matter Indirect Detection*, in *Community Summer Study 2013: Snowmass on the Mississippi*, 10, 2013 [[1310.7040](#)].
- [18] J.M. Gaskins, *A review of indirect searches for particle dark matter*, *Contemp. Phys.* **57** (2016) 496 [[1604.00014](#)].
- [19] FERMI-LAT, DES collaboration, *Searching for Dark Matter Annihilation in Recently Discovered Milky Way Satellites with Fermi-LAT*, *Astrophys. J.* **834** (2017) 110 [[1611.03184](#)].
- [20] S. Colafrancesco, M. Regis, P. Marchegiani, G. Beck, R. Beck, H. Zechlin et al., *Probing the nature of Dark Matter with the SKA*, *PoS AASKA14* (2015) 100 [[1502.03738](#)].
- [21] CTA collaboration, *Pre-construction estimates of the Cherenkov Telescope Array sensitivity to a dark matter signal from the Galactic centre*, [2007.16129](#).
- [22] MAGIC, FERMI-LAT collaboration, *Limits to Dark Matter Annihilation Cross-Section from a Combined Analysis of MAGIC and Fermi-LAT Observations of Dwarf Satellite Galaxies*, *JCAP* **02** (2016) 039 [[1601.06590](#)].
- [23] FERMI-LAT collaboration, *The Fermi Galactic Center GeV Excess and Implications for Dark Matter*, *Astrophys. J.* **840** (2017) 43 [[1704.03910](#)].
- [24] T. Bringmann and C. Weniger, *Gamma Ray Signals from Dark Matter: Concepts, Status and Prospects*, *Phys. Dark Univ.* **1** (2012) 194 [[1208.5481](#)].
- [25] M. Cirelli, *Status of Indirect (and Direct) Dark Matter searches*, *PoS ICRC2015* (2016) 014 [[1511.02031](#)].
- [26] L. Bergstrom, T. Bringmann, M. Eriksson and M. Gustafsson, *Gamma rays from Kaluza-Klein dark matter*, *Phys. Rev. Lett.* **94** (2005) 131301 [[astro-ph/0410359](#)].
- [27] L. Bergstrom, T. Bringmann, M. Eriksson and M. Gustafsson, *Two photon annihilation of Kaluza-Klein dark matter*, *JCAP* **04** (2005) 004 [[hep-ph/0412001](#)].
- [28] L. Bergstrom, T. Bringmann, M. Eriksson and M. Gustafsson, *Gamma rays from heavy neutralino dark matter*, *Phys. Rev. Lett.* **95** (2005) 241301 [[hep-ph/0507229](#)].
- [29] T. Bringmann, L. Bergstrom and J. Edsjo, *New Gamma-Ray Contributions to Supersymmetric Dark Matter Annihilation*, *JHEP* **01** (2008) 049 [[0710.3169](#)].
- [30] T. Bringmann, F. Calore, G. Vertongen and C. Weniger, *On the Relevance of Sharp Gamma-Ray Features for Indirect Dark Matter Searches*, *Phys. Rev. D* **84** (2011) 103525 [[1106.1874](#)].
- [31] S. Colafrancesco, S. Profumo and P. Ullio, *Multi-frequency analysis of neutralino dark matter annihilations in the Coma cluster*, *Astron. Astrophys.* **455** (2006) 21 [[astro-ph/0507575](#)].
- [32] S. Colafrancesco, S. Profumo and P. Ullio, *Detecting dark matter WIMPs in the Draco dwarf: A multi-wavelength perspective*, *Phys. Rev. D* **75** (2007) 023513 [[astro-ph/0607073](#)].
- [33] ANTARES collaboration, *Search for dark matter towards the Galactic Centre with 11 years of ANTARES data*, *Phys. Lett. B* **805** (2020) 135439 [[1912.05296](#)].

- [34] C. Karwin, S. Murgia, T.M.P. Tait, T.A. Porter and P. Tanedo, *Dark Matter Interpretation of the Fermi-LAT Observation Toward the Galactic Center*, *Phys. Rev. D* **95** (2017) 103005 [[1612.05687](#)].
- [35] H.E.S.S. collaboration, *Dark matter searches toward the Galactic Centre halo with H.E.S.S.*, in *52nd Rencontres de Moriond on Very High Energy Phenomena in the Universe*, pp. 255–262, 2017 [[1711.08634](#)].
- [36] V. Vitale and A. Morselli, *Indirect Search for Dark Matter from the center of the Milky Way with the Fermi-Large Area Telescope*, [0912.3828](#).
- [37] SUPER-KAMIOKANDE collaboration, *Indirect search for dark matter from the Galactic Center and halo with the Super-Kamiokande detector*, *Phys. Rev. D* **102** (2020) 072002 [[2005.05109](#)].
- [38] M. Regis and P. Ullio, *Multi-wavelength signals of dark matter annihilations at the Galactic center*, *Phys. Rev. D* **78** (2008) 043505 [[0802.0234](#)].
- [39] A. McDaniel, T. Jeltema and S. Profumo, *Multiwavelength analysis of annihilating dark matter as the origin of the gamma-ray emission from M31*, *Phys. Rev. D* **97** (2018) 103021 [[1802.05258](#)].
- [40] A. Paul, D. Majumdar and A. Dutta Banik, *Signatures of synchrotron radiation from the annihilation of dark matter at the Galactic Centre*, *JCAP* **05** (2019) 029 [[1812.10791](#)].
- [41] FERMI-LAT collaboration, *Indirect Search for Dark Matter from the center of the Milky Way with the Fermi-Large Area Telescope*, in *2009 Fermi Symposium*, 12, 2009 [[0912.3828](#)].
- [42] J. Petrović, P.D. Serpico and G. Zaharijas, *Millisecond pulsars and the Galactic Center gamma-ray excess: the importance of luminosity function and secondary emission*, *JCAP* **02** (2015) 023 [[1411.2980](#)].
- [43] D. Gaggero, D. Grasso, A. Marinelli, M. Taoso and A. Urbano, *Diffuse cosmic rays shining in the Galactic center: A novel interpretation of H.E.S.S. and Fermi-LAT γ -ray data*, *Phys. Rev. Lett.* **119** (2017) 031101 [[1702.01124](#)].
- [44] D. Gaggero, M. Taoso, A. Urbano, M. Valli and P. Ullio, *Towards a realistic astrophysical interpretation of the gamma-ray Galactic center excess*, *JCAP* **12** (2015) 056 [[1507.06129](#)].
- [45] I. Cholis, C. Evoli, F. Calore, T. Linden, C. Weniger and D. Hooper, *The Galactic Center GeV Excess from a Series of Leptonic Cosmic-Ray Outbursts*, *JCAP* **12** (2015) 005 [[1506.05119](#)].
- [46] E. Carlson, T. Linden and S. Profumo, *Cosmic-Ray Injection from Star-Forming Regions*, *Phys. Rev. Lett.* **117** (2016) 111101 [[1510.04698](#)].
- [47] M. Kuhlen, *The Dark Matter Annihilation Signal from Dwarf Galaxies and Subhalos*, *Adv. Astron.* **2010** (2010) 162083 [[0906.1822](#)].
- [48] A. Drlica-Wagner, *Searching for dwarf spheroidal galaxies and other galactic dark matter substructures with the Fermi large area telescope*, other thesis, 2013, [10.2172/1245111](#).

- [49] M. Mateo, *Dwarf galaxies of the Local Group*, *Ann. Rev. Astron. Astrophys.* **36** (1998) 435 [[astro-ph/9810070](#)].
- [50] J. Grcevich and M.E. Putman, *HI in Local Group Dwarf Galaxies and Stripping by the Galactic Halo*, *Astrophys. J.* **696** (2009) 385 [[0901.4975](#)].
- [51] B. Willman, M.R. Blanton, A.A. West, J.J. Dalcanton, D.W. Hogg, D.P. Schneider et al., *A New Milky Way companion: Unusual globular cluster or extreme dwarf satellite?*, *Astron. J.* **129** (2005) 2692 [[astro-ph/0410416](#)].
- [52] SDSS collaboration, *A New Milky Way Dwarf Satellite in Canes Venatici*, *Astrophys. J. Lett.* **643** (2006) L103 [[astro-ph/0604354](#)].
- [53] SDSS collaboration, *Cats and Dogs, Hair and A Hero: A Quintet of New Milky Way Companions*, *Astrophys. J.* **654** (2007) 897 [[astro-ph/0608448](#)].
- [54] B.P. Laevens et al., *Sagittarius II, Draco II and Laevens 3: Three new Milky way Satellites Discovered in the Pan-starrs 1 3π Survey*, *Astrophys. J.* **813** (2015) 44 [[1507.07564](#)].
- [55] B.P.M. Laevens et al., *A New Faint Milky Way Satellite Discovered in the Pan-STARRS1 3π Survey*, *Astrophys. J. Lett.* **802** (2015) L18 [[1503.05554](#)].
- [56] DES collaboration, *Eight New Milky Way Companions Discovered in First-Year Dark Energy Survey Data*, *Astrophys. J.* **807** (2015) 50 [[1503.02584](#)].
- [57] D. Kim and H. Jerjen, *A Hero's Little Horse: Discovery of a Dissolving Star Cluster in Pegasus*, *Astrophys. J.* **799** (2015) 73 [[1411.3063](#)].
- [58] D. Kim and H. Jerjen, *Horologium II: a Second Ultra-faint Milky Way Satellite in the Horologium Constellation*, *Astrophys. J. Lett.* **808** (2015) L39 [[1505.04948](#)].
- [59] S.E. Koposov, V. Belokurov, G. Torrealba and N.W. Evans, *Beasts of the Southern Wild: Discovery of nine Ultra Faint satellites in the vicinity of the Magellanic Clouds*, *Astrophys. J.* **805** (2015) 130 [[1503.02079](#)].
- [60] D. Kim, H. Jerjen, D. Mackey, G.S. Da Costa and A.P. Milone, *A Hero's Dark Horse: Discovery of an Ultra-faint Milky way Satellite in Pegasus*, *Astrophys. J. Lett.* **804** (2015) L44 [[1503.08268](#)].
- [61] D. Kim, H. Jerjen, D. Mackey, G.S. Da Costa and A.P. Milone, *KIM 3: An Ultra-faint Star Cluster in the Constellation of Centaurus*, *Astrophys. J.* **820** (2016) 119 [[1512.03530](#)].
- [62] D. Kim, H. Jerjen, A.P. Milone, D. Mackey and G.S. Da Costa, *Discovery of a Faint Outer Halo Milky Way Star Cluster in the Southern Sky*, *Astrophys. J.* **803** (2015) 63 [[1502.03952](#)].
- [63] N.F. Martin et al., *Hydra II: a faint and compact Milky Way dwarf galaxy found in the Survey of the Magellanic Stellar History*, *Astrophys. J. Lett.* **804** (2015) L5 [[1503.06216](#)].
- [64] S.E. Koposov, J. Yoo, H.-W. Rix, D.H. Weinberg, A.V. Maccio and J. Miralda-Escude, *A quantitative explanation of the observed population of Milky Way satellite galaxies*, *Astrophys. J.* **696** (2009) 2179 [[0901.2116](#)].

- [65] N. Evans, F. Ferrer and S. Sarkar, *A 'Baedeker' for the dark matter annihilation signal*, *Phys. Rev. D* **69** (2004) 123501 [[astro-ph/0311145](#)].
- [66] V. Bonnavard et al., *Dark matter annihilation and decay in dwarf spheroidal galaxies: The classical and ultrafaint dSphs*, *Mon. Not. Roy. Astron. Soc.* **453** (2015) 849 [[1504.02048](#)].
- [67] M. Winter, G. Zaharijas, K. Bechtol and J. Vandenbroucke, *Estimating the GeV Emission of Millisecond Pulsars in Dwarf Spheroidal Galaxies*, *Astrophys. J. Lett.* **832** (2016) L6 [[1607.06390](#)].
- [68] A. Kar, S. Mitra, B. Mukhopadhyaya and T.R. Choudhury, *Heavy dark matter particle annihilation in dwarf spheroidal galaxies: radio signals at the SKA telescope*, *Phys. Rev. D* **101** (2020) 023015 [[1905.11426](#)].
- [69] J. Cembranos, A. De La Cruz-Dombriz, V. Gammaldi and M. Méndez-Isla, *SKA-Phase 1 sensitivity to synchrotron radio emission from multi-TeV Dark Matter candidates*, *Phys. Dark Univ.* **27** (2020) 100448 [[1905.11154](#)].
- [70] M.T. Arun, D. Choudhury and D. Sachdeva, *Universal Extra Dimensions and the Graviton Portal to Dark Matter*, *JCAP* **10** (2017) 041 [[1703.04985](#)].
- [71] H.E.S.S. collaboration, *Search for dark matter signals towards a selection of recently detected DES dwarf galaxy satellites of the Milky Way with H.E.S.S.*, *Phys. Rev. D* **102** (2020) 062001 [[2008.00688](#)].
- [72] S. Hoof, A. Geringer-Sameth and R. Trotta, *A Global Analysis of Dark Matter Signals from 27 Dwarf Spheroidal Galaxies using 11 Years of Fermi-LAT Observations*, *JCAP* **02** (2020) 012 [[1812.06986](#)].
- [73] A. Alvarez, F. Calore, A. Genina, J. Read, P.D. Serpico and B. Zaldivar, *Dark matter constraints from dwarf galaxies with data-driven J-factors*, *JCAP* **09** (2020) 004 [[2002.01229](#)].
- [74] HAWC collaboration, *Search for gamma-ray spectral lines from dark matter annihilation in dwarf galaxies with the High-Altitude Water Cherenkov observatory*, *Phys. Rev. D* **101** (2020) 103001 [[1912.05632](#)].
- [75] A. Halder, S. Banerjee, M. Pandey and D. Majumdar, *Addressing γ -ray emissions from dark matter annihilations in 45 milky way satellite galaxies and in extragalactic sources with particle dark matter models*, *Mon. Not. Roy. Astron. Soc.* **500** (2020) 5589 [[1910.02322](#)].
- [76] FERMI-LAT, HAWC, H.E.S.S., MAGIC, VERITAS collaboration, *Combined Dark Matter searches towards dwarf spheroidal galaxies with Fermi-LAT, HAWC, HESS, MAGIC and VERITAS*, *PoS ICRC2019* (2021) 012 [[1909.06310](#)].
- [77] H.E.S.S. collaboration, *Dark Matter search with H.E.S.S. towards ultra-faint dwarf nearby DES satellites of the Milky Way*, *PoS ICRC2019* (2020) 542 [[1908.04311](#)].
- [78] J. Rico, *Gamma-Ray Dark Matter Searches in Milky Way Satellites—A Comparative Review of Data Analysis Methods and Current Results*, *Galaxies* **8** (2020) 25 [[2003.13482](#)].

- [79] P. Bhattacharjee, P. Majumdar, S. Biswas and P.S. Joarder, *Analysis of Fermi-LAT data from Tucana-II: Possible constraints on the Dark Matter models with an intriguing hint of a signal*, *JCAP* **08** (2019) 028 [[1804.07542](#)].
- [80] J. Conrad, *Statistical Issues in Astrophysical Searches for Particle Dark Matter*, *Astropart. Phys.* **62** (2015) 165 [[1407.6617](#)].
- [81] FERMI-LAT collaboration, *Observations of Milky Way Dwarf Spheroidal galaxies with the Fermi-LAT detector and constraints on Dark Matter models*, *Astrophys. J.* **712** (2010) 147 [[1001.4531](#)].
- [82] T. Sjostrand, S. Mrenna and P.Z. Skands, *A Brief Introduction to PYTHIA 8.1*, *Comput. Phys. Commun.* **178** (2008) 852 [[0710.3820](#)].
- [83] P. Gondolo, J. Edsjo, P. Ullio, L. Bergstrom, M. Schelke and E. Baltz, *DarkSUSY: Computing supersymmetric dark matter properties numerically*, *JCAP* **07** (2004) 008 [[astro-ph/0406204](#)].
- [84] T.E. Jeltema and S. Profumo, *Fitting the Gamma-Ray Spectrum from Dark Matter with DMFIT: GLAST and the Galactic Center Region*, *JCAP* **0811** (2008) 003 [[0808.2641](#)].
- [85] S. Funk, *Indirect Detection of Dark Matter with gamma rays*, *Proc. Nat. Acad. Sci.* **112** (2015) 2264 [[1310.2695](#)].
- [86] J.F. Navarro, C.S. Frenk and S.D. White, *A Universal density profile from hierarchical clustering*, *Astrophys. J.* **490** (1997) 493 [[astro-ph/9611107](#)].
- [87] A. Burkert, *The Structure of dark matter halos in dwarf galaxies*, *IAU Symp.* **171** (1996) 175 [[astro-ph/9504041](#)].
- [88] P. Salucci, M.I. Wilkinson, M.G. Walker, G.F. Gilmore, E.K. Grebel, A. Koch et al., *Dwarf spheroidal galaxy kinematics and spiral galaxy scaling laws*, *Mon. Not. Roy. Astron. Soc.* **420** (2012) 2034 [[1111.1165](#)].
- [89] J.E. Gunn and I. Gott, J. Richard, *On the Infall of Matter into Clusters of Galaxies and Some Effects on Their Evolution*, *Astrophys. J.* **176** (1972) 1.
- [90] N. Evans, J. Sanders and A. Geringer-Sameth, *Simple J-Factors and D-Factors for Indirect Dark Matter Detection*, *Phys. Rev. D* **93** (2016) 103512 [[1604.05599](#)].
- [91] T. Jeltema and S. Profumo, *Searching for Dark Matter with X-ray Observations of Local Dwarf Galaxies*, *Astrophys. J.* **686** (2008) 1045 [[0805.1054](#)].
- [92] A.B. Pace and L.E. Strigari, *Scaling Relations for Dark Matter Annihilation and Decay Profiles in Dwarf Spheroidal Galaxies*, *Mon. Not. Roy. Astron. Soc.* **482** (2019) 3480 [[1802.06811](#)].
- [93] A. McDaniel, T. Jeltema, S. Profumo and E. Storm, *Multiwavelength Analysis of Dark Matter Annihilation and RX-DMFIT*, *JCAP* **09** (2017) 027 [[1705.09384](#)].
- [94] FERMI-LAT collaboration, *Searching for Dark Matter Annihilation from Milky Way Dwarf*

- Spheroidal Galaxies with Six Years of Fermi Large Area Telescope Data*, *Phys. Rev. Lett.* **115** (2015) 231301 [[1503.02641](#)].
- [95] FERMI-LAT collaboration, *Dark Matter Constraints from Observations of 25 Milky Way Satellite Galaxies with the Fermi Large Area Telescope*, *Phys. Rev. D* **89** (2014) 042001 [[1310.0828](#)].
- [96] P. Bhattacharjee, P. Majumdar, M. Das, S. Das, P.S. Joarder and S. Biswas, *Multiwavelength analysis of low surface brightness galaxies to study possible dark matter signature*, *Mon. Not. Roy. Astron. Soc.* **501** (2021) 4238 [[1911.00369](#)].
- [97] A. Boyarsky, O. Ruchayskiy, D. Iakubovskiy, A.V. Maccio' and D. Malyshev, *New evidence for dark matter*, [0911.1774](#).
- [98] J.F. Navarro, A. Ludlow, V. Springel, J. Wang, M. Vogelsberger, S.D. White et al., *The Diversity and Similarity of Cold Dark Matter Halos*, *Mon. Not. Roy. Astron. Soc.* **402** (2010) 21 [[0810.1522](#)].
- [99] J. Wagner, *Cosmic structures from a mathematical perspective 1. Dark matter halo mass density profiles*, *Gen. Rel. Grav.* **52** (2020) 61 [[2002.00960](#)].
- [100] W.J.G. de Blok, S.S. McGaugh and V.C. Rubin, *High-resolution rotation curves of low surface brightness galaxies. II. mass models*, *The Astronomical Journal* **122** (2001) 2396.
- [101] FERMI-LAT collaboration, *The Large Area Telescope on the Fermi Gamma-ray Space Telescope Mission*, *Astrophys. J.* **697** (2009) 1071 [[0902.1089](#)].
- [102] FERMI-LAT collaboration, *Constraining Dark Matter Models from a Combined Analysis of Milky Way Satellites with the Fermi Large Area Telescope*, *Phys. Rev. Lett.* **107** (2011) 241302 [[1108.3546](#)].
- [103] A. Geringer-Sameth and S.M. Koushiappas, *Exclusion of canonical WIMPs by the joint analysis of Milky Way dwarfs with Fermi*, *Phys. Rev. Lett.* **107** (2011) 241303 [[1108.2914](#)].
- [104] W. Cash, *Parameter estimation in astronomy through application of the likelihood ratio*, *Astrophys. J.* **228** (1979) 939.
- [105] J. Mattox et al., *The Likelihood Analysis of EGRET Data*, *Astrophys. J.* **461** (1996) 396.
- [106] FERMI-LAT collaboration, *Fermi Large Area Telescope Fourth Source Catalog*, *Astrophys. J. Suppl.* **247** (2020) 33 [[1902.10045](#)].
- [107] O. Helene, *Determination of the upper limit of a peak area*, *Nucl. Instrum. Meth. A* **300** (1991) 132.
- [108] W.A. Rolke, A.M. Lopez and J. Conrad, *Limits and confidence intervals in the presence of nuisance parameters*, *Nucl. Instrum. Meth. A* **551** (2005) 493 [[physics/0403059](#)].
- [109] R. Barbieri, S. Ferrara and C.A. Savoy, *Gauge Models with Spontaneously Broken Local Supersymmetry*, *Phys. Lett. B* **119** (1982) 343.

- [110] J. Hisano, M. Kawasaki, K. Kohri, T. Moroi, K. Nakayama and T. Sekiguchi, *Cosmological constraints on dark matter models with velocity-dependent annihilation cross section*, *Phys. Rev. D* **83** (2011) 123511 [[1102.4658](#)].
- [111] A. Gruzinov and W. Hu, *Secondary CMB anisotropies in a universe reionized in patches*, *Astrophys. J.* **508** (1998) 435 [[astro-ph/9803188](#)].
- [112] A. Lewis, A. Challinor and A. Lasenby, *Efficient computation of CMB anisotropies in closed FRW models*, *Astrophys. J.* **538** (2000) 473 [[astro-ph/9911177](#)].
- [113] C.L. Bennett, D. Larson, J.L. Weiland, N. Jarosik, G. Hinshaw, N. Odegard et al., *Nine-year wilkinson microwave anisotropy probe (wmap) observations: Final maps and results*, *The Astrophysical Journal Supplement Series* **208** (2013) 20.
- [114] PLANCK collaboration, *Planck 2018 results. VI. Cosmological parameters*, [1807.06209](#).
- [115] K. Spekkens, B.S. Mason, J.E. Aguirre and B. Nhan, *A Deep Search for Extended Radio Continuum Emission From Dwarf Spheroidal Galaxies: Implications for Particle Dark Matter*, *Astrophys. J.* **773** (2013) 61 [[1301.5306](#)].
- [116] M. Regis, L. Richter, S. Colafrancesco, S. Profumo, W.J.G. de Blok and M. Massardi, *Local Group dSph radio survey with ATCA – II. Non-thermal diffuse emission*, *Mon. Not. Roy. Astron. Soc.* **448** (2015) 3747 [[1407.5482](#)].
- [117] Chyzy, K. T. and Wezgowiec, M. and Beck, R. and Bomans, D. J., *Magnetic fields in Local Group dwarf irregulars*, *A&A* **529** (2011) A94 [[1101.4647](#)].
- [118] E. Carretti, R.M. Crocker, L. Staveley-Smith, M. Haverkorn, C. Purcell, B.M. Gaensler et al., *Giant magnetized outflows from the centre of the milky way*, *Nature* **493** (2013) 66–69 [[1301.0512](#)].
- [119] M. Regis, S. Colafrancesco, S. Profumo, W. de Blok, M. Massardi and L. Richter, *Local Group dSph radio survey with ATCA (III): Constraints on Particle Dark Matter*, *JCAP* **10** (2014) 016 [[1407.4948](#)].
- [120] M. Regis, L. Richter and S. Colafrancesco, *Dark matter in the Reticulum II dSph: a radio search*, *JCAP* **07** (2017) 025 [[1703.09921](#)].
- [121] A. Natarajan, J.E. Aguirre, K. Spekkens and B.S. Mason, *Green Bank Telescope Constraints on Dark Matter Annihilation in Segue I*, [1507.03589](#).
- [122] W. Webber, M. Lee and M. Gupta, *Propagation of cosmic-ray nuclei in a diffusing galaxy with convective halo and thin matter disk*, *Astrophys. J.* **390** (1992) 96.
- [123] E.A. Baltz and J. Edsjo, *Positron propagation and fluxes from neutralino annihilation in the halo*, *Phys. Rev. D* **59** (1998) 023511 [[astro-ph/9808243](#)].
- [124] D. Maurin, F. Donato, R. Taillet and P. Salati, *Cosmic rays below $z=30$ in a diffusion model: new constraints on propagation parameters*, *Astrophys. J.* **555** (2001) 585 [[astro-ph/0101231](#)].

- [125] H. Intema, P. Jagannathan, K. Mooley and D. Frail, *The GMRT 150 MHz All-sky Radio Survey: First Alternative Data Release TGSS ADR1*, *Astron. Astrophys.* **598** (2017) A78 [[1603.04368](#)].
- [126] J.J. Condon, W.D. Cotton, E.W. Greisen, Q.F. Yin, R.A. Perley, G.B. Taylor et al., *The NRAO VLA Sky Survey*, *Astron. J* **115** (1998) 1693.
- [127] A. Weltman et al., *Fundamental physics with the Square Kilometre Array*, *Publ. Astron. Soc. Austral.* **37** (2020) e002 [[1810.02680](#)].
- [128] R. Braun, A. Bonaldi, T. Bourke, E. Keane and J. Wagg, *Anticipated SKA1 Science Performance*, .
- [129] R. Braun, A. Bonaldi, T. Bourke, E. Keane and J. Wagg, *Anticipated performance of the square kilometre array – phase 1 (ska1)*, [1912.12699](#).
- [130] M. Di Mauro, X. Hou, C. Eckner, G. Zaharijas and E. Charles, *Search for γ -ray emission from dark matter particle interactions from Andromeda and Triangulum Galaxies with the Fermi Large Area Telescope*, *Phys. Rev. D* **99** (2019) 123027 [[1904.10977](#)].
- [131] G. Beck, *Radio-Frequency Searches for Dark Matter in Dwarf Galaxies*, *Galaxies* **7** (2019) 16 [[2007.01689](#)].
- [132] CTA CONSORTIUM collaboration, *Science with the Cherenkov Telescope Array*, [1709.07997](#).
- [133] M. Vollmann, *Universal profiles for radio searches of dark matter in dwarf galaxies*, [2011.11947](#).
- [134] H. Baumgardt and S. Mieske, *High mass-to-light ratios of UCDs - Evidence for dark matter ?*, *Mon. Not. Roy. Astron. Soc.* **391** (2008) 942 [[0809.2783](#)].
- [135] S.E. Kposov et al., *Kinematics and chemistry of recently discovered Reticulum 2 and Horologium 1 dwarf galaxies*, *Astrophys. J.* **811** (2015) 62 [[1504.07916](#)].
- [136] E.N. Kirby, J.D. Simon and J.G. Cohen, *Spectroscopic Confirmation of the Dwarf Galaxies Hydra II and Pisces II and the Globular Cluster Laevens 1*, *Astrophys. J.* **810** (2015) 56 [[1506.01021](#)].
- [137] N.F. Martin et al., *Is Draco II one of the faintest dwarf galaxies? First study from Keck/DEIMOS spectroscopy*, *Mon. Not. Roy. Astron. Soc.* **458** (2016) L59 [[1510.01326](#)].
- [138] D. Kim, H. Jerjen, M. Geha, A. Chiti, A.P. Milone, D. Mackey et al., *Portrait of a Dark Horse: a Photometric and Spectroscopic Study of the Ultra-faint Milky way Satellite Pegasus iii*, *Astrophys. J.* **833** (2016) 16 [[1608.04934](#)].
- [139] DES collaboration, *Farthest Neighbor: The Distant Milky Way Satellite Eridanus II*, *Astrophys. J.* **838** (2017) 8 [[1611.05052](#)].
- [140] E.N. Kirby, J.G. Cohen, J.D. Simon, P. Guhathakurta, A.O. Thygesen and G.E. Duggan, *Triangulum II. not especially dense after all*, *The Astrophysical Journal* **838** (2017) 83.

- [141] M.G. Walker, M. Mateo, E.W. Olszewski, S. Koposov, V. Belokurov, P. Jethwa et al., *Magellan/m2fs spectroscopy of tucana 2 and grus 1*, *The Astrophysical Journal* **819** (2016) 53.
- [142] M.G. Walker, M. Mateo, E.W. Olszewski, J.I. Bailey III, S.E. Koposov, V. Belokurov et al., *Magellan/M2FS Spectroscopy of the Reticulum 2 Dwarf Spheroidal Galaxy*, *Astrophys. J.* **808** (2015) 108 [1504.03060].
- [143] DES collaboration, *Nearest Neighbor: The Low-Mass Milky Way Satellite Tucana III*, *Astrophys. J.* **838** (2017) 11 [1610.05301].
- [144] G. Torrealba, S.E. Koposov, V. Belokurov, M. Irwin, M. Collins, M. Spencer et al., *At the survey limits: discovery of the Aquarius 2 dwarf galaxy in the VST ATLAS and the SDSS data*, *Monthly Notices of the Royal Astronomical Society* **463** (2016) 712 [<https://academic.oup.com/mnras/article-pdf/463/1/712/18472890/stw2051.pdf>].
- [145] MAGLITES collaboration, *Ships Passing in the Night: Spectroscopic Analysis of Two Ultra-faint Satellites in the Constellation Carina*, *Astrophys. J.* **857** (2018) 145 [1802.06810].
- [146] M.L.M. Collins, E.J. Tollerud, D.J. Sand, A. Bonaca, B. Willman and J. Strader, *Dynamical evidence for a strong tidal interaction between the Milky Way and its satellite, Leo V*, *Mon. Not. Roy. Astron. Soc.* **467** (2016) 573 [1608.05710].
- [147] A. Genina and M. Fairbairn, *The Potential of the Dwarf Galaxy Triangulum II for Dark Matter Indirect Detection*, *Mon. Not. Roy. Astron. Soc.* **463** (2016) 3630 [1604.00838].